Progress In Electromagnetics Research M, Vol. 139, 44–68, 2026

PIER M

(Received 24 December 2025, Accepted 22 April 2026, Scheduled 12 August 2026)

Reconfigurable Intelligent Surfaces toward 6G: Technologies, Applications, and Open Challenges

Nur H. Marzuki[1], Muzammil Jusoh[1,2,*], Thennarasan Sabapathy[1], Mohamed N. Osman[1], Muhammad R. Kamarudin[3], Samer S. Albawri[4], and Cihat Seker[5]

[1]*Advanced Computing Engineering (ACE), Centre of Excellence, Universiti Malaysia Perlis, Malaysia*
[2]*Faculty of Electronic Engineering Technology, Universiti Malaysia Perlis, Pauh Putra 02600, Malaysia*
[3]*Faculty of Electrical and Electronic Engineering, Universiti Tun Hussein Onn Malaysia, Malaysia*
[4]*Space Science Centre, Climate Change Institute, Universiti Kebangsaan Malaysia, Bangi, Malaysia*
[5]*Electrical and Electronics Engineering Department, Faculty of Engineering and Architecture, Izmir Bakircay University, Turkey*

ABSTRACT: Reconfigurable Intelligent Surfaces (RISs) have emerged as a disruptive technology with the potential to fundamentally transform 5G and future 6G wireless communication systems. By intelligently controlling electromagnetic (EM) wave propagation through large arrays of reconfigurable meta-atoms, RIS enables dynamic beam shaping, interference mitigation, coverage enhancement, and energy-efficient communication. This paper presents a comprehensive review of RIS technology, focusing on its fundamental principles, classification, architectural design considerations, and diverse reconfiguration mechanisms. Key aspects, including unit cell structures, material advancements, operating modes, spatial resolution, and control strategies, are examined in detail to provide a holistic understanding of RIS functionality. The review further explores RIS performance modelling, electromagnetic simulation techniques, prototyping methods, and measurement approaches used in evaluating real-world deployments. Emerging application scenarios, including mmWave/THz communications, indoor localization, wireless power transfer, UAV-assisted networks, and smart radio environments, are also highlighted to demonstrate RIS's versatility in next-generation networks. Finally, the paper identifies existing challenges, potential limitations, and future research directions that must be addressed to realize RIS-enabled intelligent wireless ecosystems fully. The insights presented herein aim to guide researchers and industry practitioners in advancing RIS technology as a key enabler for the evolution of future 6G communication systems.

1. INTRODUCTION

The advent of fifth generation (5G) technology has ushered in a new era of connectivity, promising unprecedented data speeds, ultra-low latency, and enhanced network capacity [1–6]. As the demand for higher data rates and more reliable communication continues to escalate, the telecommunications industry is actively seeking innovative solutions to optimize the performance of 5G networks [7, 8]. However, the goals of sixth-generation (6G) wireless communication systems are expected to be revolutionary and transformative, enabling applications such as connected intelligence and providing data-driven, instantaneous, ultra-massive, and ubiquitous wireless connectivity [9], as well as ultra-efficient, high-capacity, and secure wireless systems [10].

RISs, also known as dynamically reconfigurable metasurfaces [11–16], large intelligent surfaces (LISs) [17–20], reflectarray antenna [21–33], intelligent reflecting surfaces (IRSs) [10, 19, 34–37], coding metasurface [38–46], reflective metasurface or transmissive metasurface [16], are surfaces with an array of tiny metamaterial layers [47] that allow the incident signals to be reconfigured. The array of tiny metamaterial layers is also referred to as a unit cell [48, 49], a meta-atom [50–52], or an element [53]. In this paper, the characteristics and design of unit cells are discussed. RIS consists of a two-dimensional array of reflective elements that manipulate incoming signals by adjusting their phase and amplitude without requiring external power, thereby enhancing signal quality and coverage at a cost-effective price [11, 54–58]. RISs are often made with a conformal geometry, have a low profile, and are lightweight and compact [57], and simple to deploy and remove from surfaces such as walls, ceilings, building facades, and advertisement panels [59, 60].

RIS technologies represent a key paradigm for creating intelligent radio environments. Practical implementations of RIS will likely rely extensively on metasurfaces, which are composed of metamaterials that have recently been effectively applied to commercial antenna design for satellite and terrestrial communications. This creates new opportunities for application and presents new signal-processing challenges related to utilizing the partially controlled channel [61].

RIS can reradiate and enhance the propagation of an electromagnetic field in a specific phase state [53, 62]. This enables electronic phase control [53, 62], and spectrum management without the need for traditional phase shifters [62–65]. RIS can support full-duplex (FD) [66, 67] transmission via reflections from electromagnetic waves. RIS-enhanced wireless networks operate in conjunction with existing hardware [68] and

* Corresponding author: Muzammil Jusoh (muzammil@unimap.edu.my).

TABLE 1. Comparison of representative RIS surveys and the contribution of this review.

Ref.	Main Scope	Primary Focus
[72]	RIS technologies and challenges	Practical design and deployment problems
[73]	Emphasizes RIS operating in the THz spectrum	Tuneable functions, polarization modulation and tuning mechanisms
[74]	A benchmarking framework designed to compare RIS performance	Offer method for identifying the best candidate unit cell for a given set of requirements
[71]	State-of-the-art of RIS-assisted technologies	Identify challenges in RIS implementation and potential opportunities to overcome
[70]	Perspectives and insights from an industry R&D point of view	Discussing related use cases, technical requirements, implementation challenges, and practical factors for optimizing RIS deployment
[75]	Challenges and solutions for RIS design	Hardware aspect of the RIS
This review	RIS technology	RIS fundamental principles, unit cell structure, performance modelling and measurement approaches

can also perform wireless transceiver functions by sharing data, adjusting host parameters, and processing baseband and radio-frequency (RF) signals via universal software radio peripherals (USRP) [53]. RIS is a promising technique for expanding wireless coverage [65] even if RISs are far from the base station and mobile user. Studies have shown that RIS can significantly enhance communication performance by optimizing signal reflection and improving coverage in challenging environments, such as urban areas with obstacles [58].

There are several methods for reconfiguring RIS, including electronic, optical, mechanical, and material-based approaches. RIS can also be classified into non-active (passive) and active types. Passive RIS, in this context, means no embedded component in the RIS design, while active RIS is the opposite of a passive type. Each serves a distinct role in enhancing wireless communication systems. The RISs can also be made programmable digitally by adding electronic devices, such as tuning elements and field-programmable gate arrays (FPGAs), which can be controlled digitally to provide a variety of diverse capabilities.

Passive RIS primarily manipulates incident electromagnetic waves through adjustable phase shifts without requiring energy. This makes RIS more energy-efficient and cost-effective for applications like 5G and 6G networks. Study [69] states that each coding unit cell in a passive RIS can be treated as a passive element. In contrast, active RIS incorporates components that dynamically adjust their properties, enabling more sophisticated signal processing and improved performance in complex environments. This duality enables the optimization of wireless channels and enhances overall network performance by adapting to varying conditions and user demands [70, 71].

This paper aims to provide a comprehensive analysis of reconfigurable intelligent surface (RIS) unit-cell designs and RIS patterns that enable beam-pattern reconfigurability within the 5G/6G frequency bands. It concentrates on RIS architecture, in terms of unit-cell design, RIS pattern, reconfigurable method, and substrate layers. Factors to consider before designing the unit cell include operational modes, performance targets, resolution, and application. The challenges of designing RIS also need to be considered, along with methods to overcome them, techniques to enhance RIS performance, and evaluation as the final step of RIS development. The review begins with an introductory section. The second section explains the RIS operation mode. The third section focuses on the factors that need to be considered in the RIS development process, while the fourth section highlights the challenges and enhancement features of RIS. The fifth section discusses RIS assessment, presenting various methods for measuring RIS. A measurement setup is established, either with or without Line of Sight (LoS) obstruction, and applicable to both outdoor and indoor environments. The measurement methodology varies depending on the specific RIS application, including whether it is a relay or an access point (AP). Measurement setups are available for various beam-angle device excitations and for far-field radiation-pattern measurements. Finally, the last section provides the conclusion. Table 1 presents a comparison of representative RIS surveys alongside the contributions of this review.

2. RIS OPERATION

Fundamentally, the RIS comprises discrete unit cells (passive metasurfaces), as shown in Figure 1, each with a distinct amplitude and phase response curve. For active RIS, active/lump components are embedded within passive metasurfaces [73]. In contrast, passive RIS architecture contains no embedded active/lump components. Each unit cell can individually force the incoming signal to undergo the necessary phase shift. RIS is referred to as an intelligent surface due to its ability to manipulate the polarization, bandwidth, amplitude, and phase of the incident signal.

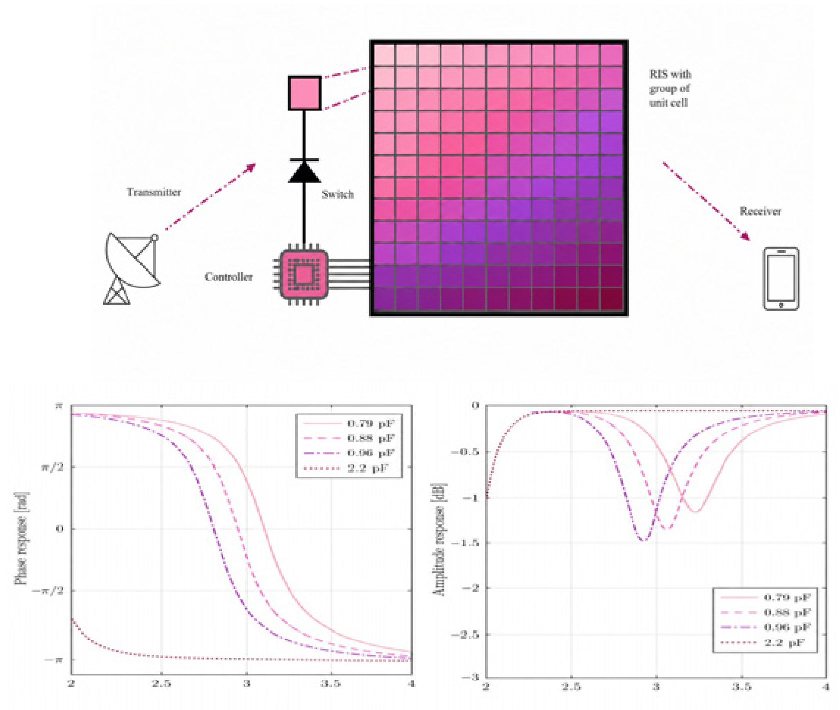

FIGURE 1. RIS operation diagram [61].

The controller and switch embedded within the unit cell determine which phase to use for each unit cell or group of unit cells. Thus, software/controller can be used to modify the entire RIS's mode, either absorption, reflection, transmission, simultaneous transmissive and reflective, refraction, focusing, polarization conversion [76], collimation, splitting/scattering, analog processing, or diffraction throughout time. These paths consist of a wireless channel to an RIS unit cell, filtering within the unit cell, and a wireless channel to the receiver.

The RIS hardware implementation with an active component relies on the concept of a metasurface, composed of digitally programmable, two-dimensional (2D) metamaterials [60, 77]. The metasurface has an electrical thickness of the order of a subwavelength at the relevant operating frequency, comprising a vast number of elements or unit cells, also known as meta-atoms [50]. The geometry, form, size/dimension (number of unit cells), orientation, arrangement, and switches of each element can be appropriately designed to adjust each one's unique signal response [60, 78, 79]. The main technical features of RIS are a reconfigurable artificial two-dimensional metasurface, passive regulation, abnormal regulation, channel cascading, and AI-driven operation.

2.1. Operation Mode

RIS can be integrated with switching elements to manipulate the incident signal. The RIS can be categorized by its operating mode. The operation modes include reflection [10, 16, 73, 77–80], transmission [16, 76, 84], Simultaneous Transmission and Reflection (STAR) [16, 76, 85–102], absorption [81–83, 103–107], focusing [52], polarization conversion [76, 107], collimation, refraction/splitting/scattering [52, 76], and analog processing. This functionality is crucial for optimizing wireless communication networks, particularly in environments with complex propagation characteristics [54, 108].

To adjust the transmission, reflection, scattering, and polarization of the incident electromagnetic wave, a reconfigurable element with two positive-intrinsic-negative (PIN) diodes is proposed in article [76]. The arrangement of the unit cell array can create a multifunctional RIS. RIS can effectively reflect and transmit incident beams, scattering them as a single, dual, or quad beam, or transforming the polarization of the incident EM wave by adjusting the states of the PIN diodes in the unit cell. Figure 2 illustrates the unit-cell design, the RIS operational concept, and the results for beam transmission, reflection, and polarization. The RIS's ability to manipulate dynamic field scattering is confirmed through full-wave electromagnetic simulations, which enable six distinct functionalities. The device can conduct a wide range of electromagnetic (EM) activities, including polarization conversion, single-, dual-, or quad-beam transmission, reflection, and more, depending on the states of the tunable switches in the RIS. After detecting a change in the surroundings, the sensing unit digitizes the sensed data and sends it to a controller, such as a Field-Programmable Gate Array (FPGA) or a microcontroller unit (MCU). The proposed unit-cell design controls beam tilting, directivity, and splitting of terahertz beams, offering several unique features through various coding patterns studied in [52], as illustrated in Figure 13.

Research [82] introduces a liquid crystal (LC)-based frequency-tunable sub-terahertz absorber, as shown in Figure 3. This tunable absorber can operate as a multifunctional, intelligent surface with absorption and reflection reconfigurability for sub-terahertz wireless applications. It can have enormous adjustable absorption bandwidths and incidence angle ranges. The benefits of absorbing RIS have been analyzed;

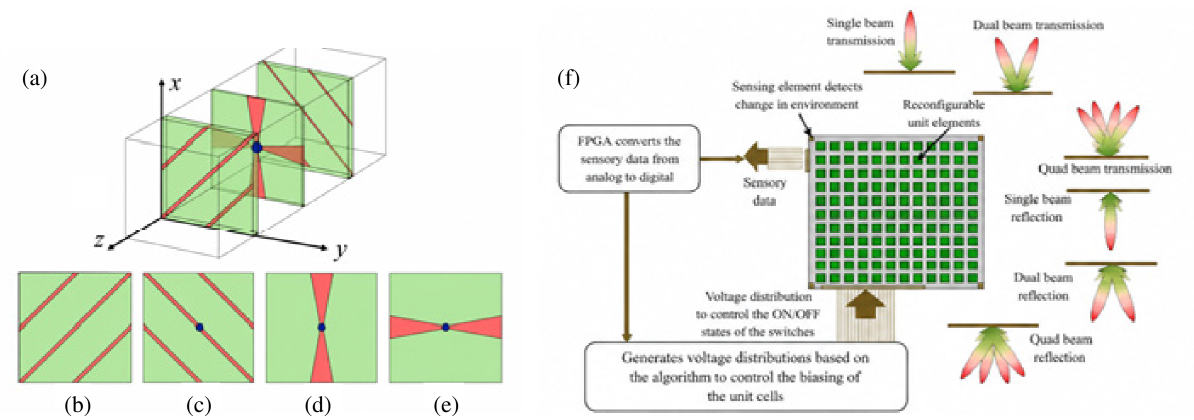

FIGURE 2. Unit cell RIS design, (a) perspective view, (b) top view of the top layer, (c) bottom view of the bottom layer, (d) top view of the middle layer, (e) bottom view of the middle layer, and (f) diagram of RIS operational concept and signal reflect and transmit beam scattering (single, dual, or quad beam) [76].

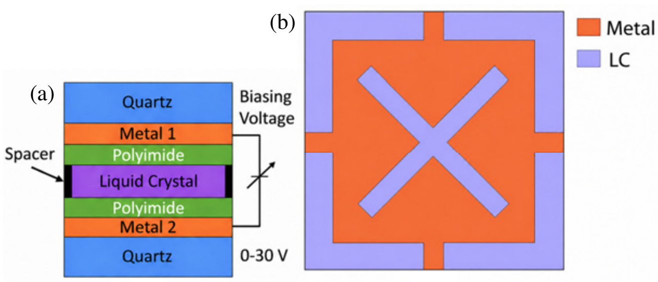

FIGURE 3. RIS with an absorber's unit cell. (a) Side view and (b) top view [82].

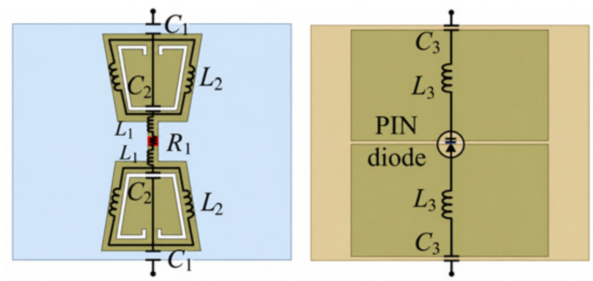

FIGURE 4. The absorptive filtering RIS unit cell structure [107].

a study [83] highlights its ability to adjust both the reflection coefficient phase and gain via absorption. The absorber RIS demonstrates significant performance improvements compared to a traditional RIS using phase-only control. Work in [109] presents an innovative, multifunctional, reconfigurable reflector unit cell engineered for the absorption, amplitude modulation, and phase modulation of incident electromagnetic waves in two polarization orientations. The technique and design of the absorbent filtering RIS are presented in [107], as shown in Figure 4.

The potential of RIS as a transmission medium is examined in [84], focusing on its use as a base access point in vehicle-to-vehicle communication systems, specifically in the context of a vehicular ad hoc network (VANET). In terms of secrecy capability, the findings demonstrate how it can be enhanced by increasing the source power, eavesdropping distance, and the number of RIS unit cells. RIS technology exhibits fading, and path loss impacts the link as the source distance increases. The average secrecy capacity is less affected by doubling the number of RIS unit cells than by doubling the source power.

3. FACTORS TO CONSIDER FOR RIS DESIGN

3.1. RIS Reconfiguration Concept

Figure 5 illustrates the classification diagram of RIS. RIS can be categorized as passive and active. Passive RIS is a simple design that does not include electronic components attached to the RIS, and reconfiguration is achieved through material design or manual adjustment of the RIS's design/topology [110, 111]. The active RIS components of a typical metamaterial-fabricated design include a controller, switches, and an array of unit cell surfaces, as shown in Figure 1. The ability of active RIS to dynamically rearrange the wireless environment after fabrication, unlike passive RIS, which remains fixed in its configuration once created, is a key difference between the two [16]. Passive reconfiguration in RIS is achieved through design methods that do not involve electronics, optics, or tunable materials, relying solely on structural or mechanical approaches. The techniques described operate independently of active components or external stimuli. They depend on established physical properties or configurations that are adjusted manually.

For active RIS, reconfigurable techniques include material-based, photonic, and electronic systems. An electronic device for switching applications involves complementary metal-oxide-semiconductor (CMOS), transistors, micro-electromechanical systems (MEMSs), PIN diodes, varactor diodes, Schottky diodes, and ferroelectric materials. Electronic reconfigurability represents the predominant and most efficient approach for managing the behavior of Reconfigurable Intelligent Surfaces (RIS). The achievement is realized through the integration of electronic switching or tuning components within each unit cell. The components alter the cell's effective impedance, resulting in a reflected wave with phase or amplitude variations.

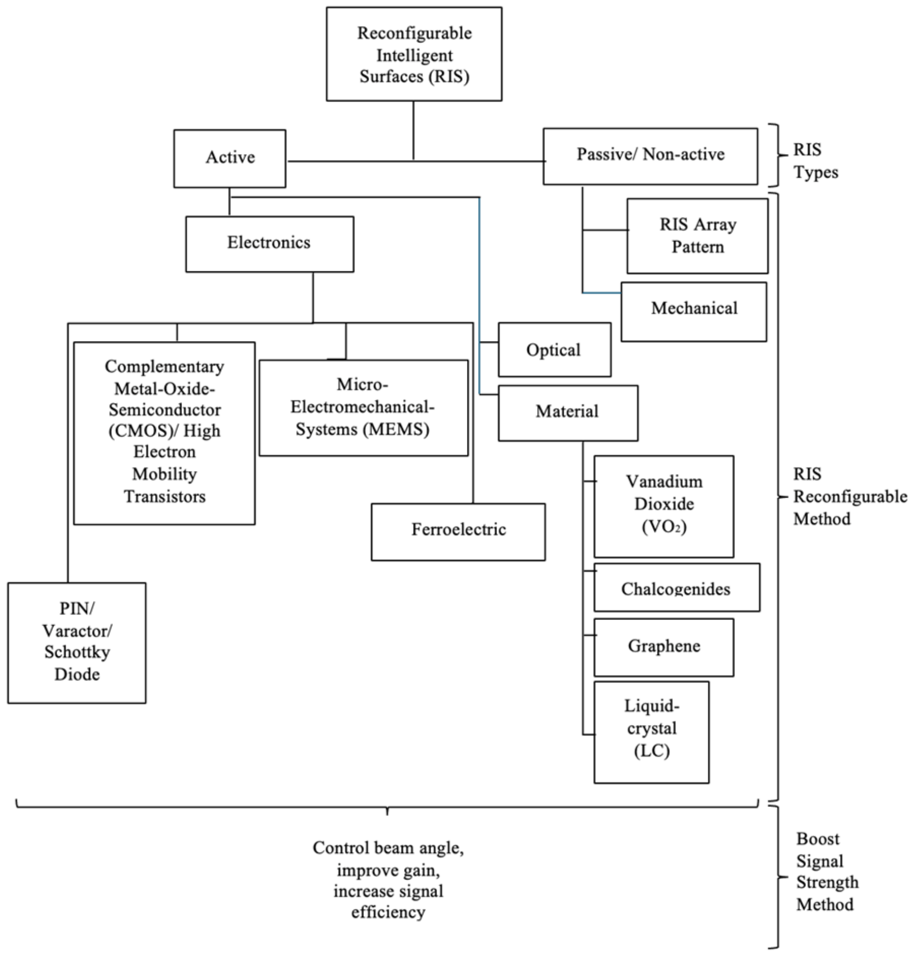

FIGURE 5. RIS classification based on the reconfiguration method.

Optically controlled RIS employs photoconductive or photo-tunable materials integrated within the unit cell to facilitate reconfigurability. The unit cell exhibits changes in electrical properties when exposed to light, attributed to fluctuations in carrier concentration or phase. This phenomenon enables real-time modulation of the reflection phase, eliminating the requirement for electrical wiring. This method facilitates rapid switching, minimizes radio-frequency (RF) loss, and enables complete wireless control, making it especially appealing for extensive, densely populated RIS installations.

The reconfigurability of RIS is determined by the selected material, such as Vanadium Dioxide (VO2), chalcogenides, graphene, liquid crystals (LC), or photoconductive films. This capability enables discrete or continuous phase tuning, which, in turn, supports flexible beam steering, wavefront shaping, and adaptive channel manipulation. RIS can be reconfigured by using materials whose electromagnetic properties change in response to external stimuli, such as voltage, light, heat, magnetic fields, or mechanical deformation. The reconfigurability of RIS is primarily influenced by the tunable material integrated within the meta-atoms. Changes in the material's electrical properties, including conductivity, permittivity (ε), and permeability (μ), result in alterations to the unit cell's resonance, facilitating dynamic control of the reflected wave.

3.1.1. Passive Reconfigurable RIS

Passive RIS was a combination of multiple unit cells/reflective elements, designed without any electronic devices that function as switches (active components) to modify the incident/input signal. A patch design is used on each unit cell, arranged to form the RIS. The unit-cell design of the passive RIS must be two or more cells to form surfaces with different phases, thereby reconfiguring the incident signal's reflection or transmission. This RIS type can modify the incident signal without a dedicated power supply, relying solely on the design's reflective element/unit cell. The number of unit cells in the design depends on the resolution setup. The RIS resolution can be set to digital or analog, and further discussion of this topic is presented in Section 3.4. In [80], a passive RIS was defined as a reflective unit cell that modifies the input signal without the need for power amplifiers. Compared with traditional relay communication systems, passive RISs exhibit greater environmental sustainability. Figures 5 and 9 illustrate the design of a passive RIS unit cell explored in the study [69].

Passive RIS has been explored by [110], where the reconfigurability of the proposed RIS is attainable through the rotation of the RIS via a mechanical motor. The unit cell served as the foundation for the RIS design. A circular patch with a radius of 10 mm was fabricated on an FR4 substrate, as illustrated in Fig-

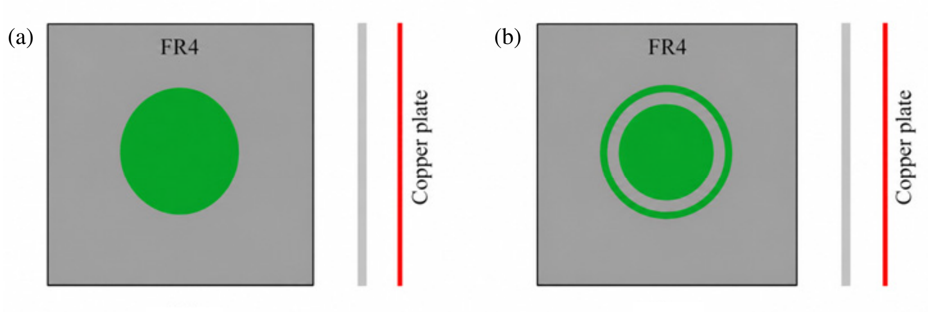

FIGURE 6. Top view and side view of the unit cell, (a) circular patch and (b) circular patch with a ring [110].

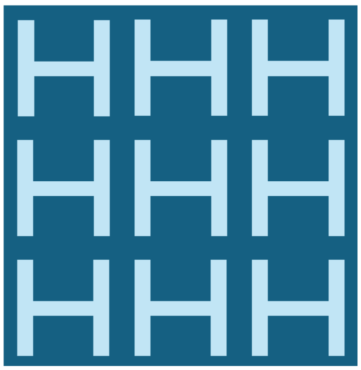

FIGURE 7. H-shaped coding element [69].

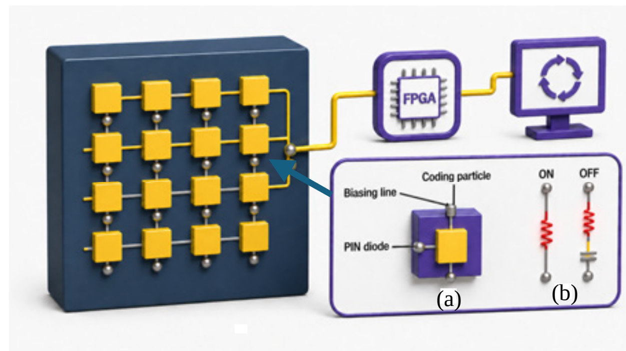

FIGURE 8. RIS fundamental architecture [62].

ure 6(a). A copper plate was positioned at the dielectric bottom to reflect the incoming waves. This type of unit cell was considered for the RIS unit-cell design due to its low cost and simplicity of manufacture. Figure 6(b) illustrates a circular patch with a circular ring design, which attains a reflection coefficient of comparable magnitude while exhibiting an approximate 180° phase shift.

Research [69] presented a "jigsaw-puzzle"-based RIS for flexible electromagnetic wave control. In the context of array antenna theory, each coding element can be considered as a passive antenna array. A detachable coding device can adjust the incidence of linear and circularly polarized waves across a broad frequency range, which is controlled by the unit-cell design. The amplitude, phase, and polarization states can be independently controlled by rearranging the unit cell design array, which comprises a 3×3 H-shaped anisotropic unit cell, as illustrated in Figure 7. A metallic H-shaped structure is etched onto a copper-backed F4B substrate.

3.1.2. Active Reconfigurable RIS

Active reconfiguration applicable to RIS involves beamforming and phase reconfiguration using tunable components or control devices [58, 80, 111, 112], with tunable components placed on each unit cell. Each unit cell in RIS accepts a single input and functions as a separate filter. It is challenging to completely isolate the RIS parts on the substrate material when they are closely spaced. The configuration of the adjacent unit cell influences each unit cell's frequency response. Figure 8 illustrates a fundamental array of unit cells on the active RIS, which is embedded with a PIN diode and a patch serving as a coding particle or reflecting unit cell, as shown in Figure 8(a). Voltage was controlled via a biasing line to switch the PIN diode 'on' or 'off', and an equivalent circuit is depicted in Figure 8(b).

There are reconfiguration techniques that can be considered for RIS design, such as a mechanical approach [48, 113, 114], electronic switch approaches (PIN diode [47, 115], varactor diodes [116], ferroelectric materials, RF PIN switches [58], complementary metal-oxide-semiconductor (CMOS) transistors-based [117, 118], Schottky diodes, high electron mobility transistors (HEMTs)), tunable materials or phase-change materials (vanadium dioxide (VO2) [119–121], chalcogenides, graphene [122, 123] and LC-base [112, 124–128]) and optical approaches (photoactive semiconductor materials) [52]).

(1) Mechanical Techniques

In [113], two surfaces were used to create a reflect array. The first surface is entirely reflective, while the other is reactive. A phase shift is applied from cell to cell to steer the reflected beam. Resonant frequency selective surface (FSS) creates a fully reflective surface on the concertina, ensuring that layer spacing is accurately maintained. In this configuration, the elements remain unchanged as the structure folds, leading to the use of dipoles. The beam-steering angle depends on the paper-folding angles shown in Figure 9.

Study [48] introduces a mechanically adjustable element. The proposed RIS element, primarily a 3D metallic cylinder with a conical element at one end, offers two mechanically reconfigurable positions, enabling 1-bit reconfiguration. The element design and two states of the element in this study are shown in Figure 10.

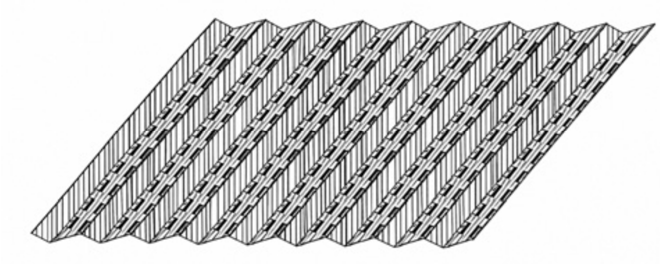

FIGURE 9. Two dipole FSS layers (Mechanical reconfiguring method) [113].

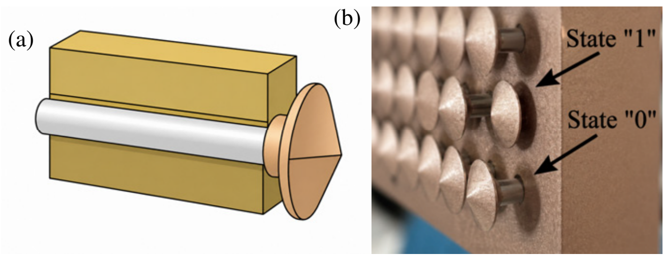

FIGURE 10. (a) 3D mechanically RIS unit cell with a cone-shaped end and (b) two states of the RIS unit cell are designated as state "0" and "1" [48].

Work in [114] proposes a numerically reflected-type dielectric metasurface architecture that would enable effective, switchable wavefront control in the terahertz range. The dielectric structures that make up the metasurfaces are hung on a metallic ground film. These structures can exhibit varying phase responses at different gap distances from one another due to the change in the Fabry-Pérot (FP) resonance. To achieve mechanically switchable beam-steering and wave-focusing responses, two unit cells are constructed. Mechanically switchable RISs have also been explored by [111], where the reconfigurability of the proposed RIS is achieved through rotation via a mechanical motor. Description of this RIS was explained in Section 3.1.1, and the RIS unit-cell design was illustrated in Figure 7.

(2) Materials Techniques

The LC-based RIS unit cell element design involved loading parallel H-shaped polygons onto two metal layers, one LC layer and three metal layers [112]. A configurable reflection phase and a reduction in the inhomogeneity effect of LC by designing an eight μm-thick LC layer as a varactor. Each element of the LC-based reflecting array is biased by square pulses generated by a microcontroller. The changes in the reflection phase eventually contribute to permittivity effects.

Furthermore, in [128], the LC offers simpler processing than the metasurface. It can achieve polarization conversion when the LC layer thickness is optimized, and low-loss LC materials are used, thereby demonstrating that the LC is non-resonant. Additionally, dynamic beam deflection switching was successfully achieved by incorporating graphene electrodes and applying an external bias to the upper and lower substrates.

In [129], a uniform bias voltage may continuously control the optical response of a range of metasurfaces based on nonuniform periodic graphene structures. A variable-focus reflecting meta-lens and a beam scanner were demonstrated, with the graphene Fermi energy consistently tuned from 0.0 to 0.9 eV. With the adjustment of the Fermi energy, the scanning beam's deflection angle varies continually while the radiation intensity stays constant. Figure 11 illustrates that the proposed RIS schematic consists of arrays of nonuniform, periodic rectangular graphene sheets.

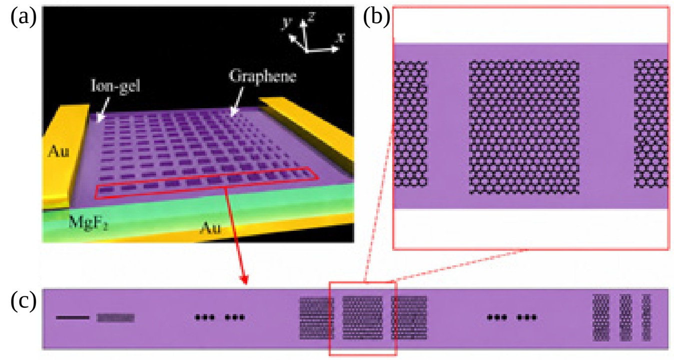

FIGURE 11. (a) RIS unit cell arrangement, (b) top view of an array of unit cells, and (c) an illustration of the unit cell with the rectangular graphene sheet [129].

(3) Electronic

A reconfigurable unit cell in [47] is developed for wideband operation by merging electric dipole resonance with magnetic dipole resonance based on the fundamental structure of the magnetoelectric dipole antenna. To alter resonances, each unit cell is integrated using a single PIN diode with 1-bit phase-shifting precision. Each unit cell is coupled to a separate bias line, allowing the operating state and reflecting phase to be managed separately.

The suggested RIS in [53] realizes 2-bit phase shifting for beamforming by combining the functionalities of radiation and phase shift on an electromagnetic surface using PIN diodes. The prototype comprises modular hardware and adaptable software, including hosts for data exchange and parameter setting, as well as radio-frequency and baseband signal processing via universal software radio peripherals (USRPs). It features signal transmission and reception via RIS.

Successful trials of a CMOS-based active tunable RIS with split-ring resonators (SRRs) in [119] show that the resonance frequency is phase- and redshifted as the applied bias voltage increases. Figure 12 illustrates the mechanism of action of RIS in conjunction with CMOS. Signal waves illuminate the electronically controlled RIS unit cell's upper side, and the applied voltage signals regulate the transmitted amplitudes and phases. Advanced electromagnetic wave regulation, such as beamforming and beam-steering devices, as well as spatial light modulation, can be realized using unit-cell arrays.

(4) Optical

In [52], Terahertz wave propagation can be optically controlled by a unit cell that integrates a metal and patterned Germanium Telluride (GeTe) on a silica substrate, providing effective modification of the incident wave's phase transition via

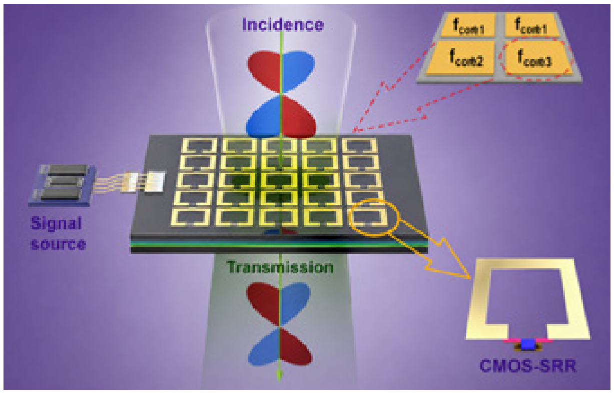

FIGURE 12. CMOS-compatible THz metamaterials [118].

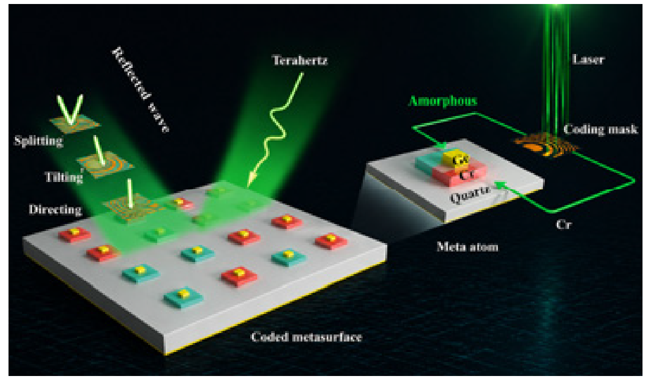

FIGURE 13. Diagram of the optical-based RIS [52].

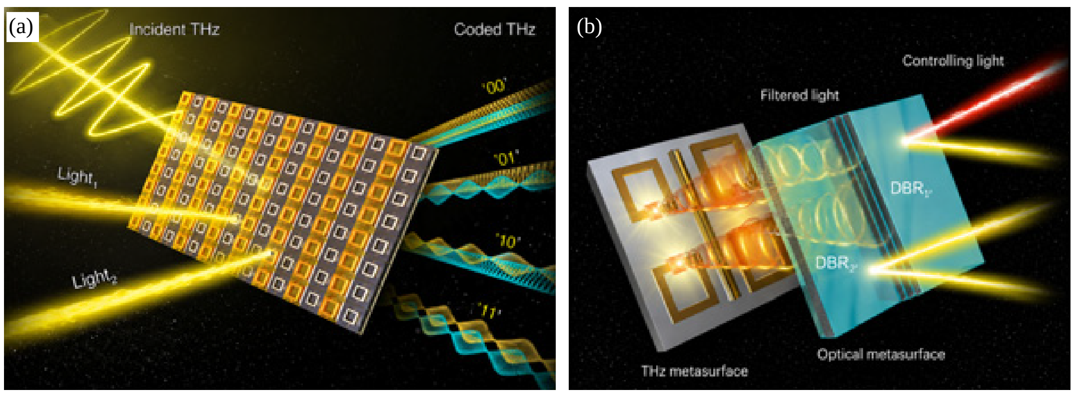

FIGURE 14. Pump laser colour-controlled RIS. (a) Two different-coloured pumped lasers regulate transmitted radiation and (b) unit cell resonating system [51].

the optical command component acting on the GeTe material state. The proposed unit-cell design is highly effective in controlling beam tilting, focusing, directivity, and splitting of terahertz beams through various coding unit-cell arrangement patterns. The specific states of each GeTe-based unit cell can be switched between crystalline (conductive) and amorphous (insulating) phases by selective UV laser irradiation with different energy-density activation. Figure 13 illustrates the optical-based approach used in RIS design.

In [51], the study combined photonic crystals with a metal unit cell to build an optically controlled 2-bit RIS. The RIS is integrated with intrinsic epitaxial silicon islands to mitigate non-radiative recombination losses, enabling ultrafast modulation. The diagram of the meta-atom/unit cell and the transmitted radiation is shown in Figure 14. Two pumped lasers with different colors can alter the transmitted terahertz radiation. The unit cell combines an organized Distributed Bragg Reflector (DBR) and a terahertz metasurface. Schematic of a one-unit cell resonating system with several connected terahertz meta-atoms and two precisely aligned DBR mirrors.

3.2. Application

RIS is commonly used as an aid in various systems and networking applications, including mm-Wave systems, multicell networks, simultaneous wireless information and power transfer networks, mobile edge computing networks, non-orthogonal multiple access (NOMA) networks, multicast networks, physical layer security (PLS) networks, Internet of Things (IoT) [57], cognitive radio networks [62], multiple-input single-output (MISO) [130] and widely used in technology connecting to wireless communication system.

RIS can also be offered as an alternative to active phased-array antennas [131], which can be deployed as a transmitter, receiver, or an aided device deployed between the transmitter and receiver to alter the wireless transmission path [132, 133]. Table 2 presents a concise comparison of RIS as alternatives to active phased arrays, tying each option to recent technology trends (5G/6G, UAV/IoT, mmWave/THz, SatCom).

By optimizing reflective beamforming, RIS enhances physical layer security by reducing information leakage, boosting the intended signal power, and suppressing interference, as discussed in [80]. This results in the creation of an 'interference-free zone' and a 'signal hotspot' within its vicinity. The possible secrecy communication rates are severely constrained when the eavesdropper's direction of travel is parallel to that of the legitimate user, or when the eavesdropper's distance from the base station (BS) is shorter than the legitimate user's. When RIS is placed close to the eavesdropper, information leakage can be minimized, as the RIS-reflected signal can be adjusted to cancel the eavesdropper's (non-RIS-reflected) BS signal.

TABLE 2. Concise comparison of RIS as an alternative to an active phased-array antenna.

Capability	Active Phased Array	RIS
Typical hardware (per element)	Full RF chain per element, Tx/Rx, phase shifter.	Unit cells, diodes/varactors, central feed or external Tx/Rx.
Power consumption	High (per-element electronics + PAs).	Low for passive RIS, higher for active and RIS with amplifiers.
Beam steering agility & precision	Very high (continuous phase control, multi-beam, fast steering).	Good for shaping/steering but often slower and discretized, improving rapidly.
Multi-beam capability	Excellent (multiple beams simultaneously possible).	Limited for fully passive and active or distributed feeds can enable more beams.
Bandwidth	Wideband possible (design dependent).	Varies (many metasurfaces are narrowband, but wideband designs exist, trend toward wider BW).
Gain/Efficiency	High (with enough active elements).	Moderate to high for large apertures, but losses possible in passive unit cells.
Complexity & cost	Highest	Low-to-moderate (control electronics and calibration add complexity)
Suitability for mmWave/THz	Excellent (widely used in mmWave radar & comms).	Strong research push for mmWave/THz metasurfaces (promising but practical limitations remain).
Typical modern use cases	Radar, high-end SatCom, military, mmWave BS.	5G/6G smart environments (coverage, blockage mitigation), low-cost beamforming surfaces, reflective relays.
Key advantages	Fast, precise, multi-beam, established tech.	Very low hardware cost per unit cell, large aperture effects, reconfigurability for environment control.

Additionally, RIS can facilitate widespread device-to-device (D2D) communication by acting as a signal-reflection hub, enabling multiple low-power transmissions to occur simultaneously through effective interference mitigation. Furthermore, RIS supports simultaneous wireless information and power transfer (SWIPT) within IoT networks, efficiently powering and connecting multiple devices. RIS also functions in an aided communication channel, combining base station-RIS and RIS-User equipment. AI can manage resources to enable an intelligent wireless environment [134].

RIS serves as a coverage extender in mm-Wave communication, which is highly susceptible to obstructions. Deploying an RIS that has clear links with the BS and the user helps circumvent the obstacle via intelligent signal reflection and thereby creates a virtual line-of-sight (LoS) link between the two when the user is situated in a dead zone where an obstacle severely blocks the direct link between it and its serving BS. RIS-aided wireless networks differ from traditional networks, which typically include only active components, including both passive (RIS) and active components (BS, AP, user terminal) [60]. RIS can also be applied to multiple-input multiple-output (MIMO) systems [135], single-input multiple-output (SIMO) systems [55], Cognitive Radio, non-orthogonal multiple access (NOMA), and two-way relaying [10].

3.3. RIS Layers

Active and passive RIS consist of multiple layers, including a radiating/parasitic/reflecting layer, a metal/conductive/copper layer, a substrate/dielectric layer [62], and a circuit board controller layer. These layers can be made from different types of material. A circuit-board controller layer is unnecessary for passive RIS, as there is no electronic device integrated into the unit cell for control. The primary focus of the study was on the radiating/parasitic layer and the dielectric layer to enhance the performance of a reconfigurable intelligent surface (RIS). Table 3 outlines the substrate used for RIS design.

A single-layer substrate is designed in Figure 15 to directly affect the incident signals, and the outer layer consists of many reflecting components printed on a dielectric substrate. A conductive panel at the bottom layer of the dielectric substrate to prevent signal/energy leakage. The layer under the copper backplane comprises a circuit board controlled by an intelligent controller, such as a field-programmable gate array (FPGA), to adjust the reflection coefficients and the phase of the RIS unit cell.

Table 4 presents the unit-cell multilayer architecture for a reconfigurable RIS. In [112], a single PIN diode is incorporated as a reconfigurable component in a 2-layer substrate. Meanwhile, [109, 133] employ a 2-layer structure with an LC material as a varactor and glass as the substrate to alter the reflection phase. In [136], a unit cell with a 4-layer substrate architecture is presented. A rectangular microstrip patch and ground are etched on the top layer of the substrate (Taconic), where two PIN diodes are soldered and connected to their biasing lines. Two middle layers are FR4 to locate the microstrip bias line to choke RF signal leakage. Two microstrip bias lines are in-

TABLE 3. RIS substrate and radiating layers.

Ref.	RIS type	Radiate Layer	Substrate/Material (relative permittivity & loss tangent)	Substrate Layers	Unit Cell
[16]	Passive	Copper	Rogers RT5880	1	2430
[110]	Passive	Copper	FR4 ($\tan\delta = 0.002$, $\varepsilon_r = 4.4$)	1	10×10
[52]	Active	Gold on top of GeTe	SiO_2	1	25×25
[121]	Active	(vanadium dioxide) VO2 & Gold	Polyimide (PI) ($\varepsilon_r = 3.5$)	1	32×32
[16]	Passive	Transparent indium tin oxide (ITO)	Glass	2	2430
[111]	Passive	Copper	Taconic TLY-5 ($\tan\delta = 0.0015$, $\varepsilon_r = 2.15$)	2	30×30
[114]	Passive	Metal	Cyclic olefin copolymer (COC, $\varepsilon_{\text{COC}} = 2.33 + 0.0016i$), air gap & silicon ($\varepsilon_{\text{Si}} = 11.9$)	2	21
[136]	Active	Metal	Glass	2	10×10
[112]	Active	Copper	Glass	2	26×38
[76]	Active	Copper	FR4 epoxy ($\varepsilon_r = 4.4$, $\tan\delta = 0.02$)	3	12×12
[137]	Active	Copper	F4BM substrate ($\varepsilon_r = 2.2$, $\tan\delta = 0.001$)	3	8×8
[138]	Active	Copper	FR4 ($\varepsilon_r = 4.3$, $\tan\delta = 0.023$)	3	20×20
[139]	Active	Copper	Taconic RF-35 ($\varepsilon_r = 3.5$, $\tan\delta = 0.0019$) & FR4 ($\varepsilon_r = 4.4$, $\tan\delta = 0.02$)	4	16×16
[140]	Active	-	FR4 & RO4350B	10	4×4

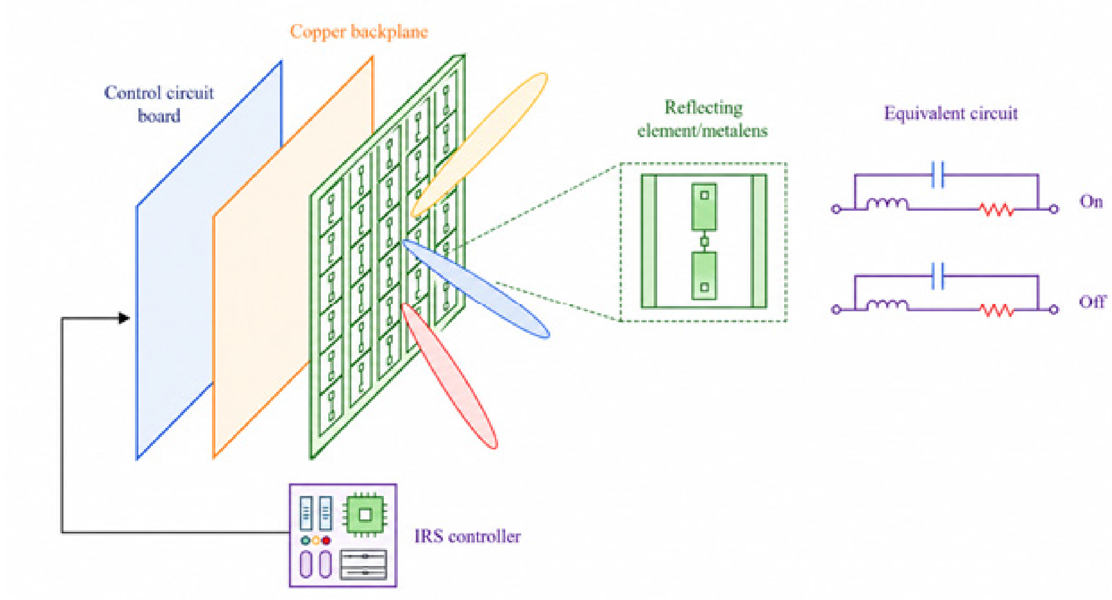

FIGURE 15. Single substrate-layer RIS architecture [60].

TABLE 4. RIS resolution (bit), switch, unit cell, and beam angle.

Ref.	Resolution (Bit)	Switch Type & No. of Switch Per Unit Cell	No. Unit Cell	Reflection Angle
[52]	1-bit	GeTe	25×25	$0°$, $40°$, $30°$ & $\pm 30°$
[58]	1-bit	1 PIN diode	16×10	$0°$, $15°$, $30°$, $45°$ & $60°$
[109]	1-bit	4 PIN diode	30×30	$10°$
[111]	1-bit	No switch	30×30	-
[138]	1-bit	4 PIN diode	20×20	$-40°$
[116]	2-bit	1 Varactor diode	32×32	$\pm 60°$
[49]	2-bit	No switch	25	Transmit $= 0°$, Reflect $= 160°$
[53]	2-bit	5 PIN diode	16×16, 800 mm $\times$ 800 mm	$\pm 60°$
[76]	2-bit	2 Pin Diode	12×12	-
[111]	2-bit	No switch	30×30	-
[111]	3-bit	No switch	30×30	-
[111]	Infinite	No switch	30×30	-

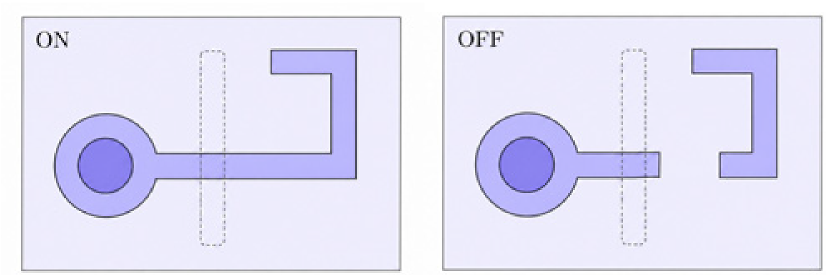

FIGURE 16. 1-bit unit cell 'off' and 'on' states [111].

stalled on the bottom FR-4 layer. Through a via for each diode, the patch's center is grounded.

3.4. RIS Resolution

Depending on the application requirements, the phase shifters on the RIS surfaces can be designed to operate at different resolutions. The surface resolution can be quantized (digital) or continuous (analog). Quantization, or digital, is a combination of two or more elemental bits, which are 1 and 0 bits. The ideal digital number for the sampled signal value at each cell in the binary algebra is determined by the appropriately ordered sequence of "0" and "1". Quantization can be categorized as 1-bit [48, 58, 109, 138, 141], 2-bit [49, 53], or n-bit (more, and can provide continuous 360° phase shifts. Binary elements "0" and "1" are mimicked based on the phase response within 0 to 2π (360°). Table 5 presents a comparison of the RIS resolution, pattern, and unit cell design. More switches must be embedded in each unit cell if larger bits are required in the RIS design, due to phase tuning between unit cells. Increasing the bit resolution of RIS will improve the elimination of the beam-splitting effect [142, 143] and reduce the quantization lobe level (QLL) and side-lobe level (SLL) [112].

3.4.1. 1-Bit

For a 1-bit RIS unit cell arrangement, "0" and "1" can be represented by phase responses of 0° and (π) 180°, respectively. For 1-bit reconfiguration resolution, the typical phase difference is π (180°) with a tolerance of 20° [48, 109, 138, 141] or 30° [76]. The magnitudes of the reflection coefficients for the on-state and off-state unit cells depend on the unit-cell design, and some designs achieve more than -0.5 dB [138] and -2.2 dB [76], respectively. The suggested unit cell has a transmission magnitude over -1.5 dB and a reflection magnitude below -1.6 dB in [76]. Figure 16 illustrates the unit-cell design for passive RIS with periodic distributions of 0° and 180°, while 'off' and 'on' conditions for a standard 1-bit unit cell. The unit cell is in 'off' condition at phase values of 0° and in 'on' condition at phase values of 180°. More RIS unit cell architectures and patterns for 1-bit resolution can be found in Tables 3 and 4. 1-bit phase quantization limits the beam-scanning resolution.

3.4.2. 2-Bit

The representations of 2-bit configuration are "00", "01", "10", and "11", which correspond to phase responses of 0, $\pi/2$, π, and $3\pi/2$, respectively. The phase responses ϕ_n are defined as $\phi_n = n\pi/2$, where $n = 0, 1, 2, 3$. Increasing the number of phase states within the range of 0° to 360° can facilitate the development of 2-bit and higher-resolution RISs. Increased resolution can mitigate the beam-splitting effect. To increase the number of phase states, PIN diodes, varactor diodes, or alternative lumped components are required to reconfigure the unit cell and modify its phase state. A 2-bit unit cell can be composed of four distinct phase states, each separated by 90° [143]. Tables 3 and 4 show the RIS unit cell architecture and the 2-bit resolution pattern.

3.4.3. 3-Bit

A 3-bit unit cell exhibiting eight distinct phase states, providing 360° coverage at 45° intervals, must be demonstrated. A configuration consisting of two D-shaped patches linked by a varactor diode enables tuning the unit cell reflection phase to 300° at 3.5 GHz, as documented in [142]. However, the passive RIS in [111] comprises eight phases organized into four pairs, representing ON and OFF states with a 180° phase difference. The specific phase pairs are $(-135°, 45°)$, $(-90°, 90°)$, $(-45°, 135°)$, and $(0°, 180°)$ for the unit-cell design, as indicated in Figure 17.

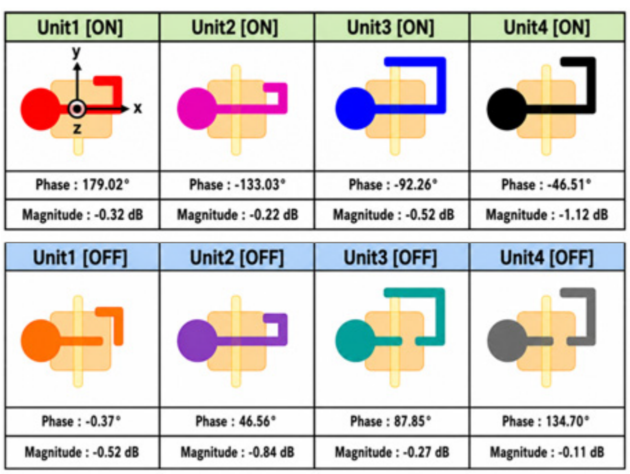

FIGURE 17. 3-bit unit-cell design and phase state [111].

3.4.4. Inhomogeneous or Infinite

There are also continuous (analog) [143] surfaces, referred to as inhomogeneous/infinite RISs [111], which may modulate electromagnetic fields more effectively than homogeneous/digitalized surfaces. The phase distribution attained optimal smoothness through the use of real representations of random phases [111]. In the context of infinite/analogue RIS resolution, the periodicity of the phase distribution is altered due to the incorporation of random phases, as illustrated in Figure 18. Inhomogeneous RISs can regulate electromagnetic fields more significantly than homogeneous ones. Figure 18 illustrates an inhomogeneous RIS via an array of nonuniform, periodic, rectangular graphene sheets.

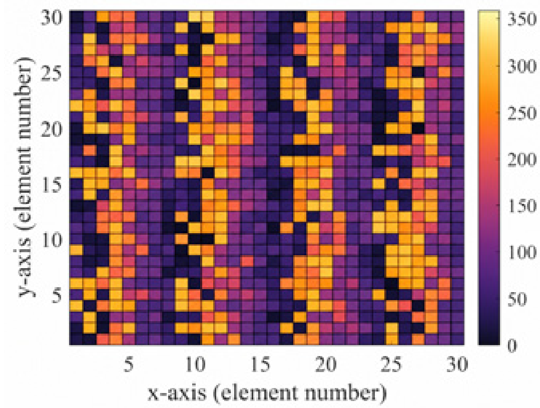

FIGURE 18. Inhomogeneous/infinite RIS phase distribution [111].

3.5. RIS Pattern

Passive RIS design must comprise two or more unit-cell designs with different phases, depending on the RIS bit resolution. The designed unit cells must be arranged into a pattern or topology to form an RIS. However, the active RIS unit-cell design phases depend on the switching condition of the same unit with the same design. A comparison of unit cell designs, RIS pattern, resolution, switch type, number of switches, number of unit cells, and reflection angle from the previous papers is presented in Table 4. The unit-cell designs can include switching more than 1 in a single unit cell. The RIS pattern depends on the phase or RIS resolution of each unit cell involved in the RIS architecture. The comparison shows that, even with more switching elements, the work in [48, 58, 109, 138, 141] is unable to achieve an improved reflection angle. The works in [48, 53, 58, 109, 138, 141] provide reflection angles up to 60°. Specifically, the design proposed in [49, 53] achieves the best reflection angle performance while using only one RF switch per unit cell.

4. RIS CHALLENGES AND ENHANCEMENT

RIS significantly enhances performance in 6G applications by dynamically altering signal propagation environments to improve key metrics, including coverage, capacity, and energy efficiency. However, there are challenges to achieving the desired performance. There are several key considerations and challenges in RIS design, including optimizing the phase shifts and amplitudes of surface elements to maximize signal-to-noise ratio (SNR) and gain, reduce interference, quantization error, mutual coupling effect, side-lobe level (SLL), quantization lobe level (QLL), and beam splitting, and mitigate multiplicative/double fading, enhancing robust beamforming capabilities and signal quality [16]. They are all phenomena that can appear in RIS design and degrade the RIS performance. Efficient resource allocation algorithms, adaptive control mechanisms, and integration with existing network infrastructure are crucial for maximizing the potential of RIS, ensuring seamless, enhanced connectivity.

A mutual coupling exists between the adjacent elements' impedances and the original element's impedance. To mitigate mutual coupling, [144] develops a scattering-parameter-based approach for RIS configuration optimization in the presence of electromagnetic mutual coupling, which has been shown to outperform current impedance-parameter-based techniques, while increasing RIS resolution can mitigate the beam-splitting effect. The method described in [145] involved dividing an RIS into multiple equal sections, referred to as tiles. Half of these tiles were then shifted by a small distance, approximately 1/8 of the wavelength, in the normal direction. This adjustment effectively suppressed quantization lobes by several decibels while maintaining the main lobe's directivity. However, it has limitations that increase the complexity of the mechanical and electrical design of RIS without offering substantial performance enhancement. In [146], it was observed that, within the xoz plane, the SLL is slightly elevated. The obstruction of the feed structure and the specular reflection of the incident wave are responsible for this issue. Additionally, the SLL experiences some degradation due to 1-bit phase quantization. As the RIS increases in size, the SLL will correspondingly decrease. Sections 4.1 and 4.2 address the difficulties and enhancements associated with multiplicative fading and signal coverage.

4.1. Multiplicative Fading

Conventionally, many reflecting unit cells are deployed at the RIS to compensate for the double-fading or multiplicative fading attenuation in the RIS-aided connection. Previous research on RIS has presented significant methods, necessitating optimization across various factors to enhance RIS technology and overcome associated problems. This results in a significant increase in circuit power consumption and a big increase in surface area. RIS with an amplifier, the incident signal is reflected and amplified by active loads (negative resistance) in each reflecting unit cell. Thus, with a given power budget at the RIS, a stronger RIS-aided connection can be obtained by amplifying the incident signal [11, 54–56, 77] and increasing the number of RIS unit cells [58, 124]. This can significantly improve system performance by boosting signal strength. The RIS hybridization with and without an amplifier can also be designed, combining the advantages of the two and facilitating enhanced cooperative transmission in wireless networks. In [140], a high-performance RIS with an amplifier is proposed that employs polarization conversion and substrate-integrated suspended line technology to effectively reduce insertion loss and noise figure.

4.1.1. Amplifying Signal

In [55, 80, 147–149], it is stated that an RIS with an amplifier consists of many reflecting units with dynamically controllable backscatter responses and that amplifying an RIS involves adding reflection amplifiers. This RIS can achieve full signal coverage, capacity gain, and an effective reduction in the number of macro base stations. Figure 19 illustrates an RIS hardware configuration. These relay-type RIS unit cells can merely reflect and amplify incident signals to improve the reflected link. Furthermore, while full-duplex amplify-and-forward relays and RIS can amplify incident signals, their hardware architectures and transmission models differ significantly.

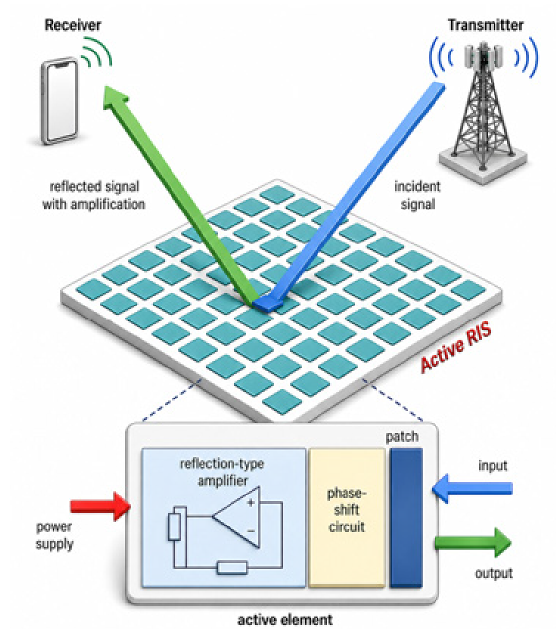

FIGURE 19. RIS with an amplifier hardware configuration [148].

A schematic representation of a tunneling reflection amplifier is shown in Figure 20. The schematic shows how the tunnel diode circuit can amplify signals in the low-power reflection amplifier. This DC-blocking capacitor blocks the low-frequency component of the input RF signal, while the RF choke inductor blocks the high-frequency component from the biasing source. The tunnel diode can work at a negative-resistance bias point with the right DC biasing source. By matching the tunnel diode's input impedance to a desired value, reflection gain stability is achieved.

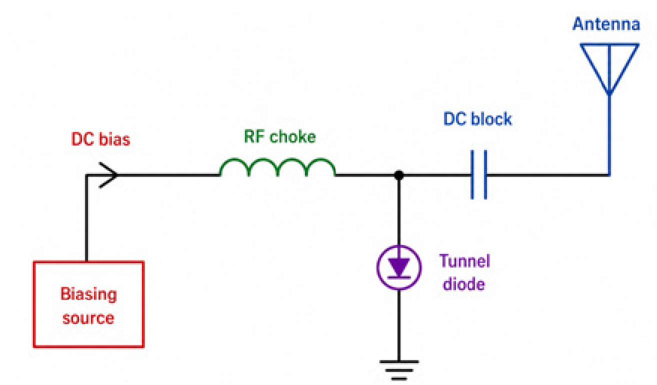

FIGURE 20. Schematic of reflection signal amplification [55].

Research in [149] presents an RIS amplifier with a sub-connected architecture to reduce its high power consumption, as shown in Figure 21. In the sub-connected architecture, multiple RIS elements within a sub-array independently control their phase shifts while sharing a single power amplifier. This differs from the fully connected architecture, where each RIS element is controlled by its own dedicated phase-shift circuit and power amplifier. This approach leads to significant power savings by reducing the number of power amplifiers required. Still, it comes at the cost of fewer controlled degrees of freedom for

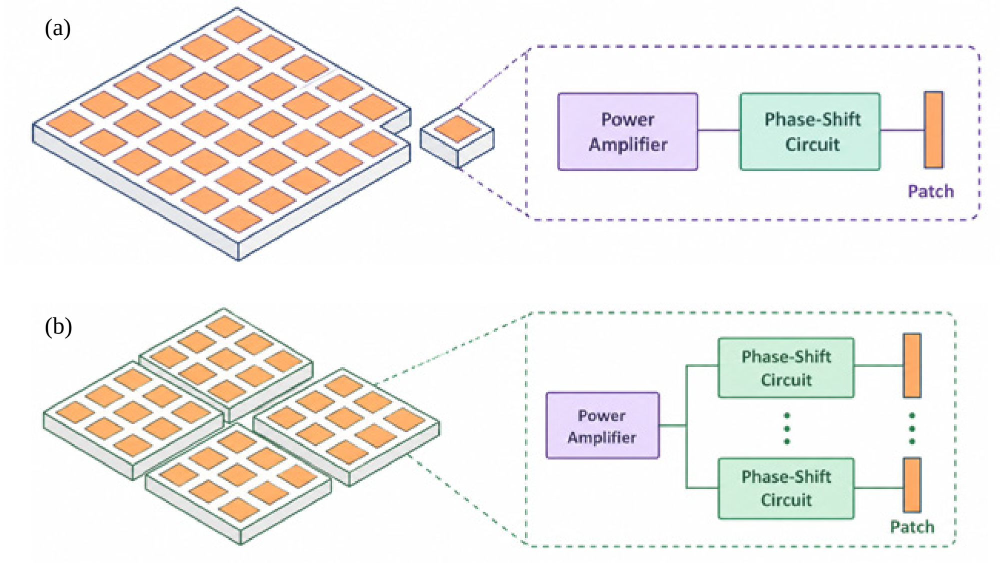

FIGURE 21. Comparison of RIS with amplifier connection architectures [149]. (a) RIS with an amplifier fully-connected architecture and (b) RIS with amplifier sub-connected architecture.

beamforming design. A dual-RIS-assisted hybrid cooperative wireless system with two non-line-of-sight paths is proposed in [11], one via RIS with an amplifier and the other via RIS without an amplifier. According to simulations, the RIS without an amplifier path exhibits higher energy efficiency under high-SNR conditions than the RIS with an amplifier channel.

When reflecting signals, active RISs with nonlinear amplifiers cause distortion. A new theorem predicting the beamforming directions of the distortion, which coincide with directions of the reflected desired signals, was developed following a research paper [150] that examined the spatial distortion characteristics throughout the far-field channel space. However, distortion can also appear in other distinct directions. It was demonstrated that the distortion spreads in multiple directions, including azimuth and elevation angles not present in the original signal, when an active RIS receives data signals from several users at different elevation angles. However, the distortion behavior in the elevation domain is independent of users' azimuth positions. Since signals broaden in the frequency domain, nonlinear distortion results in both in-band and out-of-band distortion.

The enhancement of received signal power or gain, as well as the end-to-end SNR, can be attributed primarily to an increase in the number of unit cells that can compensate for quantization loss [58, 124, 150], using discrete phase shifts (1-bit, 2-bit, or more), which experience quantization errors that reduce coherent combining efficiency. Nevertheless, even low-complexity RIS can generate meaningful SNR improvements. This method increases signal strength (gain) when the line-of-sight (LoS) link is blocked, thereby improving the received signal power. By increasing the number of RIS unit cells, it may be possible to use a lower bandwidth that would otherwise be compromised, thereby achieving improved gain. However, the SNR will also increase linearly with the number of unit cells when using conventional beamforming from an array of antennas, while narrowband capacity is maximized [151]. To remain competitive with alternative technologies, the RIS must be physically larger [152].

4.1.2. Energy Efficiency

RIS has been regarded as an innovative technology that enables high-performance, energy-efficient wireless communications [53]. In RIS with an amplifier, a multiple-input multiple-output (MIMO) system [149] is used to maximize energy efficiency. The advantages of the suggested sub-connected architecture as an energy-efficient implementation of RIS with an amplifier are confirmed by simulation results. They use an RIS with an amplifier with a sub-connected design. A sub-connected architecture significantly reduces the number of power amplifiers for power savings, at the expense of fewer degrees of freedom for beamforming design. This contrasts with a fully connected architecture, where each element integrates a dedicated power amplifier. Instead, multiple elements in the sub-connected architecture independently control their phase shifts while sharing a single power amplifier. The suggested sub-connected design is verified as an energy-efficient RIS realization with an amplifier through simulation results. The design architecture is shown in Figure 21.

According to the simulation results in [153], using a larger number of unit cells reduces the average sum power. It is suggested that adding additional reflecting unit cells to the RIS array reduces power consumption, albeit at the expense of greater computational complexity. Research [154] examines the impact of RIS location, RIS unit-cell number, base station (BS) power, and the number of users on energy efficiency. It is concluded that when users approach any installed RIS, the energy-efficiency performance reaches its peak. The rationale is that RISs reflect high-quality signals when users approach them. Therefore, adding more RISs to the cell-free (CF) network can significantly enhance energy efficiency performance while mitigating large-scale fading caused by obstructions or tall structures. As the number of passive elements increases, so does the energy-efficiency gain. The explanation is that a large number of passive components generate a coherent beam, reflecting signals with high array gain and thereby enhancing network performance. Given the low cost of the RIS elements, expanding the passive elements in the RIS unit cell might be the most cost-effective way to maximize the energy efficiency of the wideband RIS-assisted cell-free network. Energy-efficiency performance changes dramatically and keeps stable as the BS transmit power increases. It steadily declines with increasing user count, then becomes stable. A downlink wideband RIS-aided CF network is shown in Figure 22. Several RISs and BSs operate together to serve K single-antenna subscribers in the CF network.

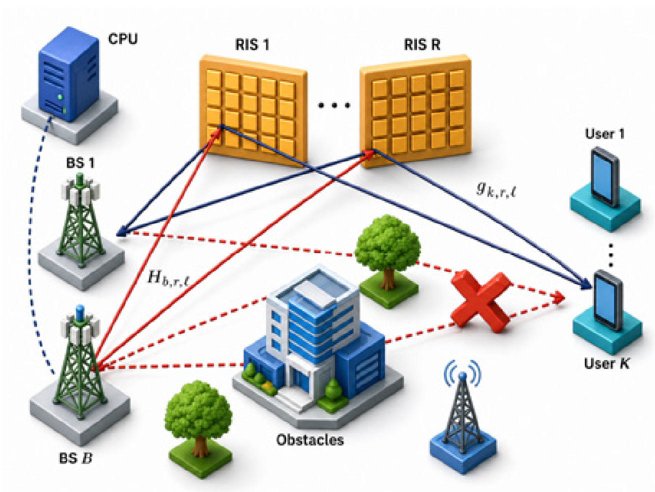

FIGURE 22. A wideband CF MIMO communication system assisted by RIS [154].

4.2. RIS Signal Coverage

4.2.1. Beam Steering and Bandwidth

Beam steering is crucial in next-generation wireless communication to improve the signal coverage. Beam steering in any direction is accomplished by adjusting the wavefront of the reflected wave coming from the RIS aperture. According to research [113], beam steering across a range of angles, from 30° to 60°, was demonstrated using linearly polarized RISs that can be screen-printed onto paper and folded into a concertina to create a reconfigurable device. In [115], a miniaturized radiating-element-based wide-angle beam-steerable RIS was demonstrated. The feed horn's placement and type were optimized to produce a low-profile arrangement with a suitable F/D ratio and location. This suggests that RIS achieves maximum aperture efficiency even at the lowest F/D. The primary cause is the well-optimized aperture efficiency, which includes feed location, reference phase, and asymmetric phase difference.

Due to the pencil-beam shape of the array factor, a large aperture has a better beam-scanning range. The measured results in [47] indicate that the proposed RIS can achieve a peak aperture efficiency, a broad gain bandwidth, and scanning angles of 0° to $+60°$ in the H-plane and $-60°$ to $+60°$ in the E-plane. The measurements in [58] verify the RIS's ability to scan over $\pm 60°$ while maintaining its single central lobe, as shown in Table 5. The theoretical design and analysis of a tunable graphene-unit-cell RIS on uneven substrates are reported in [122]. Wider operating bands and higher-frequency band selectivity can be achieved using metasurfaces with uneven substrates. A previous study [139] achieved large-angle beam scanning and independent dual-band phases. Experimental verification of two-dimensional beam-scanning performance is conducted up to a 60° scan angle.

The simulated far-field intensity distributions of the metal grating [114] are shown in Figure 23. Figures 23(a) and (b) show a large reflection beam-steering angle at a 50-µm gap distance and a small reflection beam-steering angle at a 150-µm gap distance, respectively. Figures 23(c) and (d) focus the incident beam with a small length at a 50-µm gap distance and a larger length at a 150-µm gap distance (d), respectively. The red arrow represents the incident beam, while the blue arrow indicates the output beam. The green arrows indicate the Fabry-Pérot (FP) resonances occurring at the air gaps situated between the dielectric structures and the underlying metallic film. A meta-grating method can steer the output angle over the range 19.36° to 9.54°, resulting in a 9.82° change in the deflection angle. It also focuses on the incident wave between 2 mm and 4 mm, with a gap variation of only 100 µm. The numerical simulation results also indicate that the two designs' performance aligns closely with the predictions, demonstrating high efficiency.

The comparison of the reconfiguring technique, unit cell design and number, RIS pattern, RIS resolution, and beam-steering angle is shown in Table 4. It also indicates that the number of unit cells used to form the RIS is not the primary parameter for achieving a wider steering angle, and that the maximum achievable beam-steering angle is 60°. A smaller number of unit cells can be considered for future RIS design due to cost-effectiveness, reduced complexity, and suitability for sizing.

The implementation of the RIS methodology to meet performance requirements outlined in previous research is listed in Table 5. The RIS performance focuses on the bandwidth, reflection angle (either E or H plane), gain, noise figure (NF), low reflection loss, modulation efficiency, and aperture efficiency. The complexities associated with developing the RIS methodology are substantial and entail a considerably increased number of unit cells. For passive RIS, the complexity lies in multiple unit cell designs, either on the unit cell surface or involving multiple layers of substrate or material, whereas active RIS involves parasitic or electronic elements embedded. The methodology for RIS design focused exclusively on specific performance, necessitating compromises with other factors. The performance of the RIS design cannot be fully realized as a complete system.

Table 6 summarizes the key technical challenges that hinder the practical implementation of RIS in 5G/6G wireless communication systems. It also outlines notable mitigation strategies proposed in the existing literature. The table addresses propagation and signal-level challenges, encompassing significant path loss in an entirely passive RIS, performance decline due to

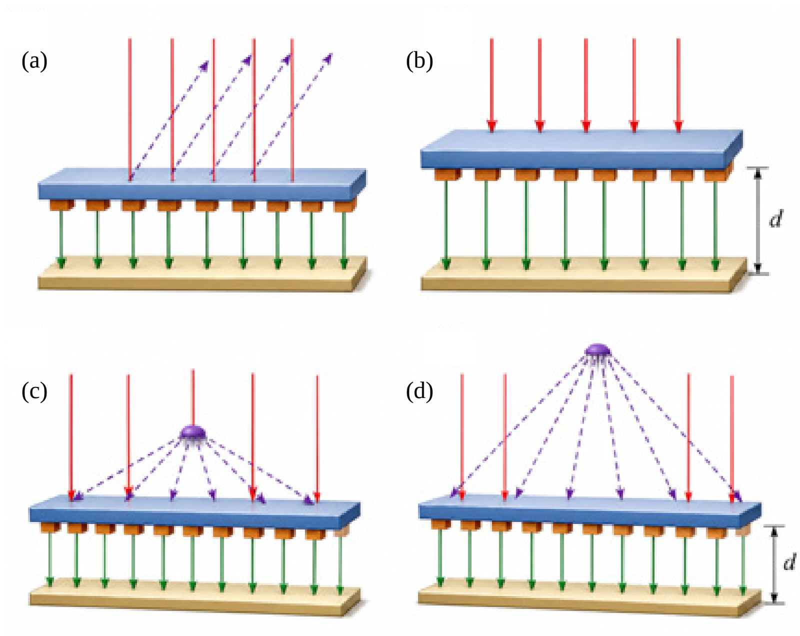

FIGURE 23. Schematics of the switchable metagrating illustrate the reflection of the incident beam at varying gap distances [114].

TABLE 5. RIS methodology and performance achievement comparison.

Ref.	**Methodology**	**Performance Achievement**	**RIS type (Reflect Angle)**	**Challenges**
[140]	Polarization conversion and substrate integrated suspended line technology	Bandwidth, reflection angle, gain, and noise figure (NF)	Active ($\pm 45^\circ$)	-
[137]	Integrated design approach combining a cavity-embedded substrate with a parasitic patch-matching layer	Bandwidth, scanning angle in both E and H-planes and low-cost	Active ($\pm 60^\circ$)	Complex design (10 substrate layer)
[16]	Selecting the proper parameters for the physical properties of the square-shaped unit cell (dielectric constant and substrate thickness)	Enhance the reflective characteristics (transmit, receive & both) and scanning angle in azimuthal plane	Passive ($\pm 45^\circ$) Active ($\pm 30^\circ$)	Reflecting both intended and interfering signals is currently a challenge for conventional RIS, which results in unwanted reflections at the receiver and deteriorates signal quality
[138]	The reflecting unit cell is an impedance-tunable, slot-based structure designed (Discrete summation of radio cross sections (RCSs))	Low reflection loss and binary phase modulation	Active (4 PIN diode /20×20) -40°	-
[57]	Modified G-S algorithm for low-complexity (1-bit passive RIS) Direct Modulation Antenna	Antenna with modulation efficiency improves system performance, phase shift keying and supports high data rates	Passive	More unit cell need for higher order QAM
[112]	The optimal random phases were implemented utilizing four pairs of unit cells with a 45° separation, based on the aperture-coupled patch, within a cost-effective PCB process.	QLL suppression, high efficiency, and a wide bandwidth are achieved across multiple reflection angles	Passive	Not electronically controlled and need plenty (unit cell design ≥ 8) for RIS develop

TABLE 6. Fundamental challenges and mitigation strategies for RIS toward 6G.

Challenge	Impact on 6G Systems	Mitigation Strategies
Severe path loss in passive RIS	Limited SNR and coverage gain	Active RIS, hybrid active-passive RIS, optimized deployment
Discrete phase quantization (1-bit/2-bit)	Quantization lobes, gain loss	Multi-bit designs, phase-optimized layouts, coding metasurfaces
Channel estimation overhead	High training complexity	Compressive sensing, cascaded channel models, ML-based estimation
Hardware non-idealities	Phase errors, efficiency degradation	Robust beamforming, hardware-aware design
Limited real-time adaptability	Reduced mobility support	Fast switching elements, low-latency control links

discrete phase quantisation, elevated channel estimation overhead, hardware imperfections, and limited real-time adaptability in the context of user mobility. Each challenge is accompanied by corresponding solutions, including active or hybrid RIS architectures, multi-bit and coding-based phase designs, compressive sensing, machine-learning-assisted channel estimation, hardware-aware beamforming, and fast reconfiguration mechanisms. These elements are presented to illustrate current research trends. The references provided serve as authoritative starting points for researchers seeking deeper technical insight. They collectively illustrate the evolution of RIS design in response to the stringent performance, scalability, and reliability requirements of future 5G and 6G networks.

5. RIS ASSESSMENT

Assessment of RIS involves evaluating their performance in simulations and real-world wireless communication environments to determine their effectiveness and potential. The RIS assessment is performed through simulation, typically using ANSYS HFSS, ADS, or CST. Furthermore, evaluations typically focus on the design and implementation aspects of RIS, examining variables such as power consumption, scalability, and compatibility with current wireless infrastructure to ensure practical relevance in forthcoming communication systems [54, 155]. The evaluation process may include simulations and measurements to predict RIS behavior and performance across diverse scenarios, and to measure key performance indicators, such as SNR, data rate, beam steering, and beamforming gains, under various conditions, thereby providing valuable insights for optimizing their deployment in next-generation wireless networks [76].

In [34], a simulation method for preventing feed blockage is demonstrated. An offset angle of the feed horn was set in the xoz plane. Paper [58] reported that a plane wave excitation can also be used in place of the feed horn antenna, and the normalized radar cross-section (RCS) pattern can be plotted from different reflection angles. In the study [141], the unit cell was developed with the high-frequency structure simulator (ANSYS HFSS). The numerical model and simulation employ the "Floquet port" boundary conditions. At this juncture, after

TABLE 7. Measurement technique for RIS in an outdoor environment.

Technique	Measurement Arrangement
Without LoS-obstructed (Outdoor) [58]	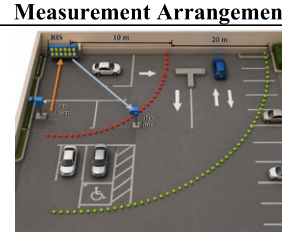
LoS-obstructed (Outdoor) [58]	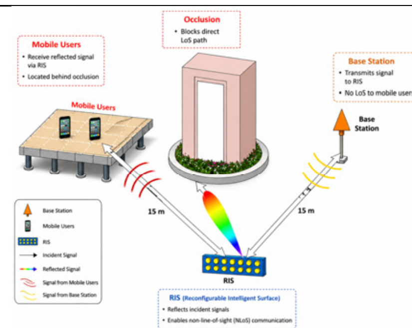
RIS as an AP for vehicular communication for PLS (Outdoor) [84]	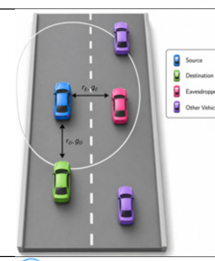
Building-mounted-RIS as relay for vehicular communication for PLS (Outdoor) [84]	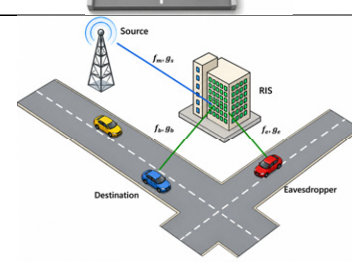

analyzing the transmission and reflection coefficients, cell adjustments were implemented until the center frequency aligned with the project's requirements. Due to the phase quantization

TABLE 8. Measurement technique for RIS in indoor environment.

Technique	Measurement Arrangement
Far-field measurement [52]	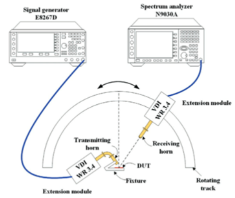
Measurement in anechoic chamber [76]	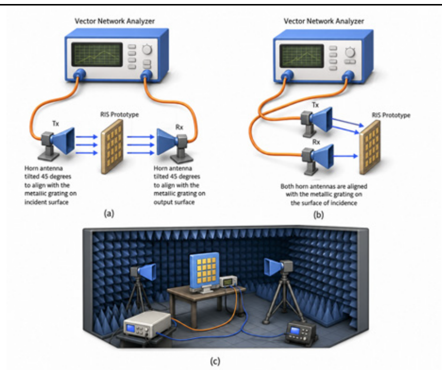
Measurement in anechoic chamber [110]	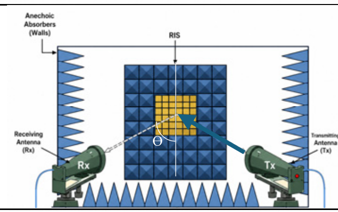
LoS-obstructed (In anechoic chamber) [124]	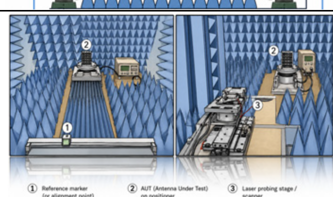
LoS-obstructed (Inside building) [124]	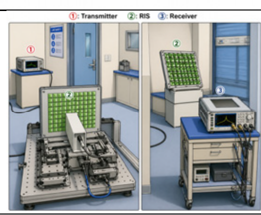
LoS-obstructed [142]	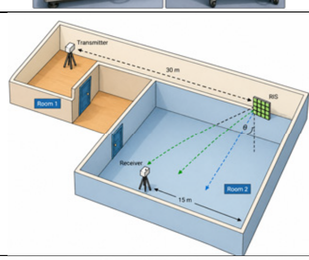
Dual-polarized RIS-based 2x2 MIMO transmission system [158]	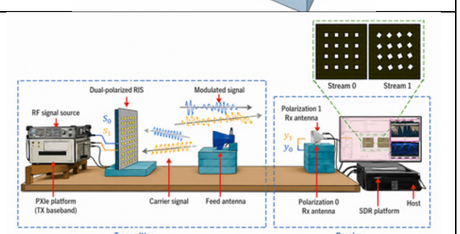

error, the reflected beam exhibits a second grating lobe at an angle opposite to the specular direction. The quantization lobes can be reduced by introducing random phase delays at each element [156, 157].

Tables 7 and 8 present the research paper pertaining to the RIS assessment. Based on the assessment, certain situations must be considered during indoor or outdoor assessments, with or without blockage. Indoor situations require a choice between an anechoic chamber and an indoor environment. The indoor environment and anechoic chamber represent performance testing in a commercial and ideal environment. The regions for antenna assessment also include factors that need to be considered, either near-field (reactive near-field or radiating near-field (Fresnel region). To analyse the various parameters of RIS, two typical horn antennas were considered. The receiver will be positioned in front of the device and moved in a circular arc. A 5G transmitter can be simulated using R&S® APS 2023 SMW200A [124]. Meanwhile, Anritsu MS2760A and vector network analyzers (VNAs) can be used to measure reflection and transmission/reflection coefficients, enabling a detailed analysis of the phase and amplitude shifts introduced by the RIS when the antennas are connected. To calculate the reflection coefficients, a horn antenna of the same type was used to measure the received powers.

5.1. Outdoor Measurement Setup

Table 7 demonstrates the configuration utilized for the outdoor evaluation of the RIS. In [58], measurements are conducted outdoors to account for real-world wave propagation phenomena, including edge diffraction, scattering from posts, and scattering from the landscape. The measurements were conducted in a parking lot (open space, no occlusions) to characterize the beamforming codebook in a real-world LoS scenario. The Universal Software Radio Peripheral (USRP) modules were attached to the feed and receiver horns, respectively. The feed horn is five meters below the surface when placed in front of the RIS. The second method in [58] involved conducting coverage measurements at the building's (occlusion) door to simulate a user scenario with severe signal loss. Utilizing an omnidirectional antenna, the receiver on the opposite side of the wall moves around the space in front of the event door. The received signal strength with and without using the RIS was compared, as the concrete wall acts as an occlusion between the transmitter and the receiver.

The secrecy capacity of RIS is studied in [84] as a crucial physical layer security (PLS) metric for a wireless vehicular network in two RIS-based vehicular-network scenarios. Two vehicular network system models were examined: one using an RIS-based access point for vehicle-to-vehicle communication and the other using a vehicular ad hoc network (VANET) with an RIS-based relay on a building as the source. RIS was compared, as the concrete wall acts as an occlusion between the transmitter and the receiver.

5.2. Indoor Measurement Setup

Table 8 illustrates the in-house measurement configuration utilized in the present study. In-house [52] measurement equipment was used to assess the performance of the manufactured prototype [52]. The platform consisted of two millimeter-wave signal generator extension modules, a spectrum analyzer, a feeding horn antenna, a receiving horn antenna, and a signal generator. A semicircle-shaped rotating track was centered on the under-test metasurface. The apparatus was mounted atop a 3D-printed structure, enabling precise customization of the incidence angle between the meta-device and the feeding antenna. The signal generator (Agilent E8267D) was modified to extend its measurement frequency range to WR 3.4 (0.22–0.33 THz domain) using an extension module (VDI WR 3.4). The extension module is fed by the signal generator. The wave output signal was fed into the transmitting horn antenna. A second extension module with a receiving horn antenna was positioned on the revolving track to identify the reflected radiating signal from the gadget.

Research [76] employs a measurement setup that utilizes a pair of horn antennas placed at the prototype's opposing ends within an anechoic chamber. The prototype is illuminated by a plane wave due to the precise spacing of the horn antennas. The prototype is secured with a window made of absorbent foam. For prototype accuracy, it must be broad and tall enough above the horn antennas to prevent signal diffraction at the sample margins. The RIS in [110] is positioned at the centre of the primary absorbing material. The goal of adding more absorbers is to reduce unwanted radiation from the outside and reflections from the room's walls, rather than using an anechoic chamber.

The performance of the RIS prototype is assessed in [124] and [142] in both indoor settings, emphasizing RIS performance in an indoor practical context, and outlines the essential design factors. The practical modification of electromagnetic waves is investigated using a planned and installed RIS to illustrate its significant impact on a wireless link. An experimental case study is described in which the receiver is positioned in the transmitter's blind spot, rendering the received signal indecipherable without incorporation of the reconfigurable intelligent surface into the link.

The dual-polarized RIS-based 2×2 MIMO transmission system prototype is shown in [158]. The feed antenna transmits a 2.7 GHz single-tone carrier signal produced by the RF signal source. A 45° angle is used for the feed antenna, and a line-polarized horn antenna is used so that both polarizations 0 and 1 have carrier components. The RIS and the feed antenna are separated by 0.8 and 1.6 meters, respectively. After down-conversion and sampling by a software-defined radio (SDR) platform, the corresponding digital baseband signals can be obtained. The receiver side uses two single-polarized antennas to receive the signals in polarizations 0 and 1. The host computer then performs baseband signal processing and demodulation.

6. CONCLUSION

The current state of the art in RIS will significantly impact communications towards 6G. Future communications will require a low-cost, self-powered RIS with multifunctional features (such as steering the beam in the desired direction and determining the direction of arrival of the incoming signal, among others). RIS will be helpful for higher-frequency communications, such as THz communications, where a LoS between the transmitter and receiver is crucial. The state of the art in RIS design clarifies that controlling components and methods have been used for beam shaping and phase reconfiguration. The components used include mechanical, semiconductor, and optical approaches, as well as tunable materials. The design of the RIS unit cell can vary to suit different application needs and operational environments. An operational environment for cell function requires reflective, transmissive, hybrid reflective-transmissive, active, frequency-selective, and polarization-selective properties. Various unit-cell architectures suit the function of the RIS, including single- and multi-layer designs, different substrate types, varying numbers of unit cells, the switching components used, and resolution.

The differences between RISs that can be found in previous research were based on their frequency, substrate, switches, number of switches, substrate and conductive layers, unit cells, patch design, unit cell topology (homogeneous, inhomogeneous, or periodic/gradient structures), RIS aperture size, feed distances, and feed angle to achieve the reflection or transmitting signal performance needed. This structure influences the reflection or transmission of a signal through wave-propagation parameters and capabilities, such as aperture efficiency, reflection coefficient, beamwidth, beam scanning (tilting, directing, or splitting), gain, side lobe level, energy efficiency, signal-to-noise ratio, fading effect, and reflection loss. Adding an amplifier to reduce multiplicative fading will consume significant power due to the additional integrated active component. This will also increase the RIS-correlated signal at the receiver.

A passive RIS consumes no power, but it is not programmable because it lacks integrated active components. The absence of power consumption signifies that no electronic components are embedded within the passive RIS, thereby eliminating the need for an external power supply during operation. Passive RIS is the simplest RIS design, offering a cost-effective, energy-saving solution. For all RIS design methods, the gain performance can be improved by increasing the RIS aperture size.

It is necessary to progress beyond a mere listing of techniques and clearly define the trade-offs and design principles that influence the practical implementation of RIS for 6G. In scenarios where low cost, ultra-low power consumption, and ease of large-scale deployment are prioritized, passive RIS should be favored, particularly for applications such as indoor coverage enhancement or in static environments. Nevertheless, it is essential to recognize the inherent challenges posed by double-fading path loss and the resulting limitations in signal-to-noise ratio (SNR). On the other hand, active or hybrid RIS configurations are more appropriate for long-range links, cell-edge users, and high-frequency systems (mmWave/THz), where SNR is crucial, though this comes with increased power consumption, degraded noise figure, and added system complexity. In terms of phase resolution, low-bit (1-bit or 2-bit) RISs offer hardware simplicity and robustness; however, they also introduce quantization lobes, gain reduction, and elevated side-lobe levels, which make them suitable for coarse beam steering. Conversely, higher-bit designs enhance beam fidelity and spectral efficiency but lead to a substantial increase in control overhead, biasing complexity, and calibration requirements. From a measurement and validation perspective, common pitfalls include neglecting feeder illumination nonuniformity, ignoring mutual coupling effects, and overestimating gain due to improper reference antenna calibration. Therefore, it is strongly recommended to conduct far-field measurements, phase-error characterization, and repeatability tests. A comprehensive performance evaluation should not depend exclusively on peak gain. It must also consider side-lobe level (SLL), beam efficiency, SNR improvement, energy efficiency (bits/Joule), and reconfiguration latency. These factors collectively provide a more comprehensive assessment of RIS effectiveness. The implementation of design-aware synthesis is essential to convert RIS's theoretical potential into a reliable technology that enables 6G advancements

Many studies have shown that RIS works well in single-link or small-array situations. However, deploying it at scale in densely populated cities, indoors, and in cell-free environments is more difficult. As the array size increases, the double-fading effect, spatial correlation across large openings, and mutual coupling among closely spaced elements become more noticeable. Future research should focus on scalable deployment, accounting for RIS density, placement height, orientation, and blockage statistics. Create hierarchical RIS architectures in which surfaces operate in coordinated clusters rather than as separate entities, and investigate element grouping and subarray-based control to reduce dimensionality, using ultra-low-latency backhaul/control links for real-time reconfiguration. Real RIS hardware is very different from models made to look perfect. Phase noise, finite switching speed, amplitude-phase coupling, bias-line parasitics, and temperature-dependent drift are all issues that need to be examined in more detail in the future. These issues lower performance, especially at mmWave and THz frequencies. Researchers should focus on RIS in 6G, which will likely work in AI-native networks that optimise environmental sensing, traffic forecasting, and beam adaptation simultaneously. For commercialisation to proceed, it needs to adopt standardised evaluation methods. Researchers should look beyond peak gain to include effective SNR improvement (including cascaded losses), energy efficiency, reconfiguration delay, beam efficiency, side-lobe suppression, and reliability when a device is moving.

ACKNOWLEDGEMENT

This work was funded by the Ministry of Higher Education through the Fundamental Research Grant Scheme (FRGS) under grant number FRGS/1/2023/TK07/UNIMAP/02/10.

REFERENCES

[1] Sudhamani, C., M. Roslee, J. J. Tiang, and A. U. Rehman, "A survey on 5G coverage improvement techniques: Issues and future challenges," *Sensors*, Vol. 23, No. 4, 2356, 2023.

[2] Nguyen, D. C., P. N. Pathirana, M. Ding, and A. Seneviratne, "Blockchain for 5G and beyond networks: A state of the art survey," *Journal of Network and Computer Applications*, Vol. 166, 102693, 2020.

[3] Shehab, M. J., I. Kassem, A. A. Kutty, M. Kucukvar, N. Onat, and T. Khattab, "5G networks towards smart and sustainable cities: A review of recent developments, applications and future perspectives," *IEEE Access*, Vol. 10, 2987–3006, 2022.

[4] Zawish, M., F. A. Dharejo, S. A. Khowaja, S. Raza, S. Davy, K. Dev, and P. Bellavista, "AI and 6G into the metaverse: Fundamentals, challenges and future research trends," *IEEE Open Journal of the Communications Society*, Vol. 5, 730–778, 2024.

[5] Westhausen, N. L. and B. T. Meyer, "Binaural multichannel blind speaker separation with a causal low-latency and low-complexity approach," *IEEE Open Journal of Signal Processing*, Vol. 5, 238–247, 2023.

[6] Lyko, T., M. Broadbent, N. Race, M. Nilsson, P. Farrow, and S. Appleby, "Improving quality of experience in adaptive low latency live streaming," *Multimedia Tools and Applications*, Vol. 83, No. 6, 15 957–15 983, 2024.

[7] Shrestha, R., K. Kerpez, C. S. Hwang, M. Mohseni, J. M. Cioffi, and D. M. Mittleman, "A wire waveguide channel for terabit-per-second links," *Applied Physics Letters*, Vol. 116, No. 13, 131102, 2020.

[8] Hajiyat, Z. R. M., A. Ismail, A. Sali, and M. N. Hamidon, "Antenna in 6G wireless communication system: Specifications, challenges, and research directions," *Optik*, Vol. 231, 166415, 2021.

[9] Saad, W., M. Bennis, and M. Chen, "A vision of 6G wireless systems: Applications, trends, technologies, and open research problems," *IEEE Network*, Vol. 34, No. 3, 134–142, 2020.

[10] Zhu, Z., Z. Liu, J. Meng, Z. Lu, Z. Li, Z. Chu, and W. Hao, "Intelligent reconfigurable surface-assisted symbiotic radio systems: Architecture, applications and challenges," *IEEE Internet of Things Magazine*, Vol. 8, No. 4, 108–115, 2025.

[11] Pandey, A. K., A. Aathmaram, and B. Sainath, "Hybrid RIS-assisted cooperative communication model design and performance analysis," in *2022 IEEE 19th Annual Consumer Communications & Networking Conference (CCNC)*, 1–6, Las Vegas, NV, USA, 2022.

[12] Li, Y., J. Wang, R. Zhu, S. Sui, Y. Han, C. Ding, T. Qiu, X. Fu, S. Wang, and S. Qu, "Reconfigurable phase-modulated metasurfaces via rotating adjustable resistor," *Results in Physics*, Vol. 47, 106378, 2023.

[13] Han, X., S. Ding, Q.-S. Jia, W.-H. Zhang, H. Tang, Q. Zhang, Z. Zhu, Y. Zhou, Z. Zhang, X. Wang, Y.-M. Huang, and B.-Z. Wang, "A versatile design method applied to reconfigurable metasurfaces," *Journal of Applied Physics*, Vol. 135, No. 8, 083303, 2024.

[14] Zhang, H., Q. Wang, M. Fink, and G. Ma, "Optimizing multi-user indoor sound communications with acoustic reconfigurable metasurfaces," *Nature Communications*, Vol. 15, No. 1, 1270, 2024.

[15] Tian, J. and W. Cao, "Reconfigurable flexible metasurfaces: From fundamentals towards biomedical applications," *PhotoniX*, Vol. 5, No. 1, 2, 2024.

[16] Ali, A., S. Danesh, Z. R. Omam, and M. Khalily, "Reconfigurable intelligent surfaces for advanced wireless networks and wave computing," in *2024 IEEE Asia-Pacific Conference on Applied Electromagnetics (APACE)*, 1–4, Langkawi, Kedah, Malaysia, 2024.

[17] Hou, T., Y. Liu, Z. Song, X. Sun, Y. Chen, and L. Hanzo, "MIMO assisted networks relying on intelligent reflective surfaces: A stochastic geometry based analysis," *IEEE Transactions on Vehicular Technology*, Vol. 71, No. 1, 571–582, 2022.

[18] Liang, Y.-C., R. Long, Q. Zhang, J. Chen, H. V. Cheng, and H. Guo, "Large intelligent surface/antennas (LISA): Making

reflective radios smart," *Journal of Communications and Information Networks*, Vol. 4, No. 2, 40–50, 2019.
[19] Chen, J., "Multi-user communications for line-of-sight large intelligent surface systems," *EURASIP Journal on Advances in Signal Processing*, Vol. 2023, No. 1, 129, 2023.
[20] Hu, S., H. Wang, and M. C. Ilter, "Design of near-field beamforming for large intelligent surfaces," *IEEE Transactions on Wireless Communications*, Vol. 23, No. 1, 762–774, 2024.
[21] Martinez-de-Rioja, D., E. Martinez-de Rioja, Y. Rodriguez-Vaqueiro, J. A. Encinar, A. Pino, M. Arias, M. Arrebola, and G. Toso, "Parabolic reflectarray antenna to generate multiple beams for geostationary high throughput satellites in Ka-band," *International Journal of Microwave and Wireless Technologies*, Vol. 15, No. 1, 15–24, 2023.
[22] Zang, J., S. Wang, J. Pan, M. Meng, Z. Wang, and S. An, "W-band large-scale high-gain filtering reflectarray antenna," *Microwave and Optical Technology Letters*, Vol. 66, No. 1, e33879, 2024.
[23] Wu, X., Z. Li, Z. Zhang, X. Wang, L. Si, and W. Zhu, "Mechanically reconfigurable folded reflectarray antenna for variable near-field focusing," *IEEE Transactions on Antennas and Propagation*, Vol. 71, No. 12, 10 038–10 043, 2023.
[24] Xu, L., X. Ge, Q. Zhang, F. Dang, P. Zhang, J. Liu, and C. Yuan, "A beam-steerable wideband reflectarray antenna for C-band high-power microwave application," *IEEE Access*, Vol. 11, 64 559–64 566, 2023.
[25] Sathyanarayanan, V., G. N. A. Mohammed, K. Savarimuthu, and M. Kanagasabai, "Wideband millimeter-wave reflectarray antenna with reduced cross-polarization," *International Journal of Microwave and Wireless Technologies*, Vol. 16, No. 4, 636–644, 2024.
[26] Guo, L., Y. Chen, and X. Chen, "A metal-only folded reflectarray antenna," *IEEE Antennas and Wireless Propagation Letters*, Vol. 22, No. 6, 1441–1445, 2023.
[27] Sangmahamad, P., P. Janpugdee, and Y. Zhao, "A metasurface-based electronically reconfigurable and dual-polarized reflectarray antenna for beam-steering applications," *IEEE Access*, Vol. 11, 137 414–137 425, 2023.
[28] Zhou, Q. and L. Guo, "A multipolarized metal-only reflectarray antenna," *IEEE Transactions on Antennas and Propagation*, Vol. 71, No. 8, 6977–6982, 2023.
[29] Yang, J., Y. Zhang, M.-C. Tang, Z. Zhang, and M. Qu, "Compact wideband FSS-absorber-based low-RCS reflectarray antenna," *Chinese Journal of Aeronautics*, Vol. 36, No. 6, 332–339, 2023.
[30] Bashir, G., A. K. Singh, and A. Dubey, "Wide band beam steering digital metasurface reflectarray antenna for millimeter wave applications," *IEEE Access*, Vol. 11, 121 800–121 810, 2023.
[31] Bashir, G., A. K. Singh, and A. Dubey, "A single layered high-gain digital metasurface reflectarray antenna for millimeter wave applications," *Microwave and Optical Technology Letters*, Vol. 66, No. 1, e33898, 2024.
[32] Xu, L., Q. Zhang, W. Yuan, *et al.*, "A high-power microwave reflectarray antenna based on variable rotation technique," *High Power Laser and Particle Beams*, Vol. 36, No. 1, 5–11, 2024.
[33] Wang, Z., R. Zhang, W. Song, X. Lin, B. Xie, J. Wang, and R. Zhao, "W-band single-layer broadband reflectarray antenna," *IEEE Access*, Vol. 11, 66 309–66 317, 2023.
[34] Wu, Q. and R. Zhang, "Towards smart and reconfigurable environment: Intelligent reflecting surface aided wireless network," *IEEE Communications Magazine*, Vol. 58, No. 1, 106–112, 2020.
[35] Cheng, Y., K. H. Li, Y. Liu, K. C. Teh, and H. V. Poor, "Downlink and uplink intelligent reflecting surface aided networks: NOMA and OMA," *IEEE Transactions on Wireless Communications*, Vol. 20, No. 6, 3988–4000, 2021.
[36] Wang, L., K. Wang, C. Pan, and N. Aslam, "Joint trajectory and passive beamforming design for intelligent reflecting surface-aided UAV communications: A deep reinforcement learning approach," *IEEE Transactions on Mobile Computing*, Vol. 22, No. 11, 6543–6553, 2023.
[37] Xia, E., B.-J. Hu, and Q. Shen, "A survey of physical layer secret key generation enhanced by intelligent reflecting surface," *Electronics*, Vol. 13, No. 2, 258, 2024.
[38] Shao, R. W., J. W. Wu, Z. X. Wang, H. Xu, H. Q. Yang, Q. Cheng, and T. J. Cui, "Macroscopic model and statistical model to characterize electromagnetic information of a digital coding metasurface," *National Science Review*, Vol. 11, No. 3, nwad299, 2024.
[39] Tang, P., X. Zheng, T. Ma, G. Cheng, G. Wu, X. Bao, H. Sun, J. Ding, and L. Si, "Terahertz dual-band dual-polarization 3-bit coding metasurface for multiple vortex beams generation," *Electronics*, Vol. 12, No. 8, 1868, 2023.
[40] Khan, H. A., C. Huang, Q. Xiao, and S. M. Abbas, "Polarization-dependent coding metasurface with switchable transmission and RCS reduction bands," *Micromachines*, Vol. 14, No. 1, 78, 2023.
[41] Zhang, Y., K. Yin, L. Liang, H. Yao, X. Yan, X. Hu, C. Huang, F. Qiu, R. Zhang, Y. Li, Y. Wang, Z. Li, and Z. Wang, "Dirac semimetal-enabled multi-bit coding metasurface for dynamic manipulation of terahertz beams," *Current Applied Physics*, Vol. 58, 21–27, 2024.
[42] Wang, S. R., J. Y. Dai, J. C. Ke, Z. Y. Chen, Q. Y. Zhou, Z. J. Qi, Y. J. Lu, Y. Huang, M. K. Sun, Q. Cheng, and T. J. Cui, "Radar micro-Doppler signature generation based on time-domain digital coding metasurface," *Advanced Science*, Vol. 11, No. 19, 2306850, 2024.
[43] Gao, L., Y. Zhou, H. Zhu, P. Zheng, J. Liu, Z. He, Z. Xu, and Y. Cui, "Reconfigurable amplitude-phase-coding metasurface with flexible beamforming capability," *Electronics*, Vol. 12, No. 22, 4565, 2023.
[44] Wang, J.-L., X.-C. Dong, L. Yin, Z.-X. Yang, H.-D. Wan, H.-M. Chen, and K. Zhong, "Vanadium dioxide based terahertz dual-frequency multi-function coding metasurface," *Acta Physica Sinica*, Vol. 72, No. 9, 098101, 2023.
[45] Liu, X., S. Li, C. He, H. Yang, and X. Cao, "Digital coding metasurface for multi-beam and multi-mode OAM in full-space," *Results in Physics*, Vol. 51, 106638, 2023.
[46] Yang, Z. X., J. L. Wang, W. J. Sun, *et al.*, "Multi-frequency and multi-beam tunable terahertz coding metasurface in full space," *Acta Optica Sinica*, Vol. 44, No. 4, 300–309, 2024.
[47] Xiang, B. J., X. Dai, and K.-M. Luk, "A wideband low-cost reconfigurable reflectarray antenna with 1-bit resolution," *IEEE Transactions on Antennas and Propagation*, Vol. 70, No. 9, 7439–7447, 2022.
[48] Baena-Molina, M., A. Palomares-Caballero, G. Martinéz-García, R. Padial-Allué, P. Padilla, and J. F. Valenzuela-Valdés, "1-bit RIS unit cell with mechanical reconfiguration at 28 GHz," in *2024 18th European Conference on Antennas and Propagation (EuCAP)*, 1–5, Glasgow, United Kingdom, 2024.
[49] Yu, H., J. Su, and Z. Li, "A reflect-transmit array with full-space independent beamforming capability," in *2021 13th International Symposium on Antennas, Propagation and EM Theory (ISAPE)*, 1–3, Zhuhai, China, 2021.

[50] Liaskos, C., S. Nie, A. Tsioliaridou, A. Pitsillides, S. Ioannidis, and I. Akyildiz, "A new wireless communication paradigm through software-controlled metasurfaces," *IEEE Communications Magazine*, Vol. 56, No. 9, 162–169, 2018.

[51] He, W., X. Cheng, S. Hu, Z. Ren, Z. Yu, S. Wan, Y. Hu, and T. Jiang, "Color coded metadevices toward programmed terahertz switching," *Light: Science & Applications*, Vol. 13, No. 1, 142, 2024.

[52] Lin, Q.-W., H. Wong, L. Huitema, and A. Crunteanu, "Coding metasurfaces with reconfiguration capabilities based on optical activation of phase-change materials for terahertz beam manipulations," *Advanced Optical Materials*, Vol. 10, No. 1, 2101699, 2022.

[53] Dai, L., B. Wang, M. Wang, X. Yang, J. Tan, S. Bi, S. Xu, F. Yang, Z. Chen, M. Di Renzo, C.-B. Chae, and L. Hanzo, "Reconfigurable intelligent surface-based wireless communications: Antenna design, prototyping, and experimental results," *IEEE Access*, Vol. 8, 45 913–45 923, 2020.

[54] Feng, Y., Q. Hu, K. Qu, W. Yang, Y. Zheng, and K. Chen, "Reconfigurable intelligent surfaces: Design, implementation, and practical demonstration," *Electromagnetic Science*, Vol. 1, No. 2, 1–21, 2023.

[55] Long, R., Y.-C. Liang, Y. Pei, and E. G. Larsson, "Active reconfigurable intelligent surface-aided wireless communications," *IEEE Transactions on Wireless Communications*, Vol. 20, No. 8, 4962–4975, 2021.

[56] Wang, W. and K. Song, "Hybrid active-passive reconfigurable intelligent surface for cooperative transmission systems," *Applied Sciences*, Vol. 14, No. 1, 231, 2024.

[57] Wei, M., S. Wang, X. Su, J. Jin, Q. Wang, and Y. Yuan, "High-order direct antenna modulation via passive reconfigurable intelligent surface," in *2024 International Conference on Future Communications and Networks (FCN)*, 1–6, Valletta, Malta, 2024.

[58] Trichopoulos, G. C., P. Theofanopoulos, B. Kashyap, A. Shekhawat, A. Modi, T. Osman, S. Kumar, A. Sengar, A. Chang, and A. Alkhateeb, "Design and evaluation of reconfigurable intelligent surfaces in real-world environment," *IEEE Open Journal of the Communications Society*, Vol. 3, 462–474, 2022.

[59] Liu, Y., X. Liu, X. Mu, T. Hou, J. Xu, M. Di Renzo, and N. Al-Dhahir, "Reconfigurable intelligent surfaces: Principles and opportunities," *IEEE Communications Surveys & Tutorials*, Vol. 23, No. 3, 1546–1577, 2021.

[60] Wu, Q. and R. Zhang, "Towards smart and reconfigurable environment: Intelligent reflecting surface aided wireless network," *IEEE Communications Magazine*, Vol. 58, No. 1, 106–112, 2020.

[61] Björnson, E., H. Wymeersch, B. Matthiesen, P. Popovski, L. Sanguinetti, and E. de Carvalho, "Reconfigurable intelligent surfaces: A signal processing perspective with wireless applications," *IEEE Signal Processing Magazine*, Vol. 39, No. 2, 135–158, 2022.

[62] Pan, C., H. Ren, K. Wang, J. F. Kolb, M. Elkashlan, M. Chen, M. Di Renzo, Y. Hao, J. Wang, A. L. Swindlehurst, X. You, and L. Hanzo, "Reconfigurable intelligent surfaces for 6G systems: Principles, applications, and research directions," *IEEE Communications Magazine*, Vol. 59, No. 6, 14–20, 2021.

[63] Di Renzo, M., A. Zappone, M. Debbah, M.-S. Alouini, C. Yuen, J. de Rosny, and S. Tretyakov, "Smart radio environments empowered by reconfigurable intelligent surfaces: How it works, state of research, and the road ahead," *IEEE Journal on Selected Areas in Communications*, Vol. 38, No. 11, 2450–2525, 2020.

[64] Yang, Y., B. Zheng, S. Zhang, and R. Zhang, "Intelligent reflecting surface meets OFDM: Protocol design and rate maximization," *IEEE Transactions on Communications*, Vol. 68, No. 7, 4522–4535, 2020.

[65] Makarfi, A. U., R. Kharel, K. M. Rabie, O. Kaiwartya, X. Li, and D.-T. Do, "Reconfigurable intelligent surfaces based cognitive radio networks," in *2021 IEEE Wireless Communications and Networking Conference Workshops (WCNCW)*, 1–6, Nanjing, China, 2021.

[66] Zhang, W., Z. Wen, C. Du, Y. Jiang, and B. Zhou, "Ris-assisted self-interference mitigation for in-band full-duplex transceivers," *IEEE Transactions on Communications*, Vol. 71, No. 9, 5444–5454, 2023.

[67] Tewes, S., M. Heinrichs, P. Staat, R. Kronberger, and A. Sezgin, "Full-duplex meets reconfigurable surfaces: RIS-assisted SIC for full-duplex radios," in *ICC 2022 — IEEE International Conference on Communications*, 1106–1111, Seoul, Korea, 2022.

[68] Zhou, S., W. Xu, K. Wang, M. Di Renzo, and M.-S. Alouini, "Spectral and energy efficiency of IRS-assisted MISO communication with hardware impairments," *IEEE Wireless Communications Letters*, Vol. 9, No. 9, 1366–1369, 2020.

[69] Wang, H., S. Sui, Y. Li, H. Chen, J. Wang, J. Zhang, and S. Qu, "Passive reconfigurable coding metasurface for broadband manipulation of reflective amplitude, phase and polarization states," *Smart Materials and Structures*, Vol. 29, No. 1, 015029, 2020.

[70] Sode, M., M. Ponschab, L. N. Ribeiro, S. Haesloop, E. Tohidi, M. Peter, S. Stańczak, B. H. Mohamed, W. Keusgen, H. Mellein, E. Yassin, and B. Schroeder, "Reconfigurable intelligent surfaces for 6G mobile networks: An industry R&D perspective," *IEEE Access*, Vol. 12, 163 155–163 171, 2024.

[71] Sharma, T., A. Chehri, and P. Fortier, "Reconfigurable intelligent surfaces for 5G and beyond wireless communications: A comprehensive survey," *Energies*, Vol. 14, No. 24, 8219, 2021.

[72] Yang, F., P. Pitchappa, and N. Wang, "Terahertz reconfigurable intelligent surfaces (RISs) for 6G communication links," *Micromachines*, Vol. 13, No. 2, 285, Feb. 2022.

[73] Singh, K., M. Saikia, K. Thiyagarajan, D. Thalakotuna, K. Esselle, and S. Kodagoda, "Multi-functional reconfigurable intelligent surfaces for enhanced sensing and communication," *Sensors*, Vol. 23, No. 20, 8561, 2023.

[74] Björnson, E., H. Wymeersch, B. Matthiesen, P. Popovski, L. Sanguinetti, and E. de Carvalho, "Reconfigurable intelligent surfaces: A signal processing perspective with wireless applications," *IEEE Signal Processing Magazine*, Vol. 39, No. 2, 135–158, 2022.

[75] Tan, X., Z. Sun, J. M. Jornet, and D. Pados, "Increasing indoor spectrum sharing capacity using smart reflect-array," in *2016 IEEE International Conference on Communications (ICC)*, 1–6, Kuala Lumpur, Malaysia, 2016.

[76] Cui, T. J., M. Q. Qi, X. Wan, J. Zhao, and Q. Cheng, "Coding metamaterials, digital metamaterials and programmable metamaterials," *Light: Science & Applications*, Vol. 3, No. 10, e218, 2014.

[77] Guo, M., Z. Lin, R. Ma, K. An, D. Li, N. Al-Dhahir, and J. Wang, "Inspiring physical layer security with RIS: Principles, applications, and challenges," *IEEE Open Journal of the Communications Society*, Vol. 5, 2903–2925, 2024.

[78] Zheng, X., W. Cheng, and J. Wang, "Huygens-Fresnel model based position-aided phase configuration for 1-bit RIS assisted wireless communication," *IEEE Transactions on Communications*, Vol. 72, No. 8, 5102–5116, 2024.

[79] Pandit, S., D. Kim, Y. Youn, D. An, and W. Hong, "Frequency-tunable absorber using liquid crystal at 140 GHz," *IEEE Antennas and Wireless Propagation Letters*, Vol. 23, No. 3, 1119–1123, 2024.

[80] Wang, F. and A. L. Swindlehurst, "Applications of absorptive reconfigurable intelligent surfaces in interference mitigation and physical layer security," *IEEE Transactions on Wireless Communications*, Vol. 23, No. 5, 3918–3931, 2024.

[81] Makarfi, A. U., K. M. Rabie, O. Kaiwartya, X. Li, and R. Kharel, "Physical layer security in vehicular networks with reconfigurable intelligent surfaces," in *2020 IEEE 91st Vehicular Technology Conference (VTC2020-Spring)*, 1–6, Antwerp, Belgium, 2020.

[82] Li, Y., J. Wang, Y. Liu, W. Xie, and J. Wang, "Weighted sum power maximization for STAR-RIS assisted SWIPT systems," in *GLOBECOM 2023 — 2023 IEEE Global Communications Conference*, 1–6, Kuala Lumpur, Malaysia, 2023.

[83] Garnepudi, M. D., U. M. Ukyam, and K. K. Gurrala, "Sum secrecy rate maximization for control jamming assisted STAR-RIS wireless network," in *2023 International Conference on Microwave, Optical, and Communication Engineering (ICMOCE)*, 1–4, Bhubaneswar, India, 2023.

[84] Toregozhin, T., M. H. N. Shaikh, and G. Nauryzbayev, "Performance analysis and enhancement through cooperative NOMA in STAR-RIS-aided systems," in *2023 International Balkan Conference on Communications and Networking (BalkanCom)*, 1–6, İstanbul, Turkiye, 2023.

[85] Yang, S., Z. Ding, and H. Zhu, "STAR-RIS aided multi-antenna NOMA downlink and uplink transmissions: A low-complexity approach," *IEEE Transactions on Wireless Communications*, Vol. 23, No. 9, 10 773–10 787, 2024.

[86] Toregozhin, T., M. H. N. Shaikh, A. Almagambetov, and G. Nauryzbayev, "Performance of STAR-RIS-aided cooperative NOMA networks under Nakagami-m fading," *Ad Hoc Networks*, Vol. 156, 103399, 2024.

[87] Wu, C., X. Mu, Y. Liu, X. Gu, and X. Wang, "Resource allocation in STAR-RIS-aided networks: OMA and NOMA," *IEEE Transactions on Wireless Communications*, Vol. 21, No. 9, 7653–7667, 2022.

[88] Gunasinghe, D., D. Kudathanthirige, and G. A. A. Baduge, "The achievable rate performance of STAR-RIS aided massive MIMO systems," *IEEE Transactions on Communications*, Vol. 72, No. 6, 3681–3700, 2024.

[89] Liu, Y., K. Huang, X. Sun, J. Yang, and J. Zhao, "Secure wireless communications for STAR-RIS-assisted millimetre-wave NOMA uplink networks," *IET Communications*, Vol. 17, No. 9, 1127–1139, 2023.

[90] Mu, X., Y. Liu, J. Xu, L. Guo, and J. Lin, "Joint beamforming optimization for simultaneously transmitting and reflecting (STAR) RIS aided communications (Invited Paper)," in *2021 55th Asilomar Conference on Signals, Systems, and Computers*, 709–714, Pacific Grove, CA, USA, 2021.

[91] Wei, W., X. Pang, C. Xing, N. Zhao, and D. Niyato, "STAR-RIS aided secure NOMA integrated sensing and communication," *IEEE Transactions on Wireless Communications*, Vol. 23, No. 9, 10 712–10 725, 2024.

[92] Wu, C., C. You, Y. Liu, X. Gu, and Y. Cai, "Channel estimation for STAR-RIS-aided wireless communication," *IEEE Communications Letters*, Vol. 26, No. 3, 652–656, 2022.

[93] Xu, J., X. Mu, and Y. Liu, "Exploiting STAR-RISs in near-field communications," *IEEE Transactions on Wireless Communications*, Vol. 23, No. 3, 2181–2196, 2024.

[94] Song, B. and F. Wang, "STAR-RIS-aided secure communications for MEC with delay/energy-constrained QoS using multi-agent deep reinforcement learning," *Ad Hoc Networks*, Vol. 154, 103370, 2024.

[95] Wen, H., A. M. T. Khel, and K. A. Hamdi, "Phase shift configuration strategies for unbalanced T&R users in STAR-RIS-aided NOMA," *IEEE Communications Letters*, Vol. 27, No. 12, 3404–3408, 2023.

[96] Shaikh, M. H. N., A. Celik, A. M. Eltawil, and G. Nauryzbayev, "Grant-free NOMA through optimal partitioning and cluster assignment in STAR-RIS networks," *IEEE Transactions on Wireless Communications*, Vol. 23, No. 8, 10 166–10 181, 2024.

[97] Gunasinghe, D. and G. Amarasuriya, "Performance analysis of STAR-RIS for wireless communication," in *ICC 2022 — IEEE International Conference on Communications*, 3275–3280, Seoul, Korea, 2022.

[98] Vu, T.-H., A. Jee, D. B. da Costa, and S. Kim, "STAR-RIS empowered NOMA systems with caching and SWIPT," *IEEE Open Journal of the Communications Society*, Vol. 5, 379–396, 2024.

[99] Mu, X., Y. Liu, L. Guo, J. Lin, and R. Schober, "Simultaneously transmitting and reflecting (STAR) RIS aided wireless communications," *IEEE Transactions on Wireless Communications*, Vol. 21, No. 5, 3083–3098, 2022.

[100] Wang, J., W. Tang, S. Jin, C.-K. Wen, X. Li, and X. Hou, "Hierarchical codebook-based beam training for RIS-assisted mmWave communication systems," *IEEE Transactions on Communications*, Vol. 71, No. 6, 3650–3662, 2023.

[101] Anam, M. K. and S. Choi, "Bowtie nanoantenna array integrated with artificial impedance surfaces for realizing high field enhancement and perfect absorption simultaneously," *IEEE Access*, Vol. 8, 99 858–99 869, 2020.

[102] Kisseleff, S., S. Chatzinotas, and B. Ottersten, "Reconfigurable intelligent surfaces in challenging environments: Underwater, underground, industrial and disaster," *IEEE Access*, Vol. 9, 150 214–150 233, 2021.

[103] Dash, S., C. Psomas, I. Krikidis, I. F. Akyildiz, and A. Pitsillides, "Active control of THz waves in wireless environments using graphene-based RIS," *IEEE Transactions on Antennas and Propagation*, Vol. 70, No. 10, 8785–8797, 2022.

[104] Hu, Q., H. Yang, X. Zeng, Y. Rao, and X. Y. Zhang, "Methodology and design of absorptive filtering reconfigurable intelligent surfaces," *IEEE Transactions on Antennas and Propagation*, Vol. 72, No. 6, 5301–5306, 2024.

[105] Alamzadeh, I., G. C. Alexandropoulos, N. Shlezinger, and M. F. Imani, "A reconfigurable intelligent surface with integrated sensing capability," *Scientific Reports*, Vol. 11, No. 1, 20737, 2021.

[106] Meng, C., F. Xue, G. Feng, H. Chen, Y. Li, and S.-W. Wong, "A multifunctional reflectarray based on resistance modulation," in *2024 15th Global Symposium on Millimeter-Waves & Terahertz (GSMM)*, 100–101, Hong Kong, 2024.

[107] Rana, B., S.-S. Cho, and I.-P. Hong, "Parameters and measurement techniques of reconfigurable intelligent surfaces," *Micromachines*, Vol. 13, No. 11, 1841, 2022.

[108] Kim, T., S. Lee, S. Oh, J. Kim, J. Oh, and S. Choi, "Prephased 1-bit reflective metasurface with optimum random phases for multiple reflection angles at 140 GHz," *TechRxiv*, 2024.

[109] Zhang, W., Y. Li, and Z. Zhang, "A reconfigurable reflectarray antenna with an 8 μm-thick layer of liquid crystal," *IEEE Transactions on Antennas and Propagation*, Vol. 70, No. 4, 2770–2778, 2022.

[110] Callaghan, P., P. Giannakou, S. G. King, M. Shkunov, and P. R. Young, "Linearly polarized reconfigurable reflectarray surface," *IEEE Transactions on Antennas and Propagation*, Vol. 69, No. 10, 6480–6488, 2021.

[111] Chen, K., X. Zhang, X. Chen, T. Wu, Q. Wang, Z. Zhang, Q. Xu, J. Han, and W. Zhang, "Active dielectric metasurfaces for switchable terahertz beam steering and focusing," *IEEE Photonics Journal*, Vol. 13, No. 1, 1–11, 2021.

[112] Lee, S.-G., Y.-H. Nam, Y. Kim, J. Kim, and J.-H. Lee, "A wide-angle and high-efficiency reconfigurable reflectarray antenna based on a miniaturized radiating element," *IEEE Access*, Vol. 10, 103 223–103 229, 2022.

[113] Da Silva, L. G., Z. Chu, P. Xiao, and A. C. Sodré Jr., "A varactor-based 1024-element RIS design for mm-waves," *Frontiers in Communications and Networks*, Vol. 4, 1086011, 2023.

[114] Venkatesh, S., X. Lu, H. Saeidi, and K. Sengupta, "A high-speed programmable and scalable terahertz holographic metasurface based on tiled CMOS chips," *Nature Electronics*, Vol. 3, No. 12, 785–793, 2020.

[115] Liu, Y., T. Sun, Y. Xu, X. Wu, Z. Bai, Y. Sun, H. Li, H. Zhang, K. Chen, C. Ruan, Y. Sun, Y. Hu, W. Zhao, T. Nie, and L. Wen, "Active tunable THz metamaterial array implemented in CMOS technology," *Journal of Physics D: Applied Physics*, Vol. 54, No. 8, 085107, 2021.

[116] Shabanpour, J., S. Beyraghi, and A. Cheldavi, "Ultrafast reprogrammable multifunctional vanadium-dioxide-assisted metasurface for dynamic THz wavefront engineering," *Scientific Reports*, Vol. 10, No. 1, 8950, 2020.

[117] Jiang, M., F. Hu, L. Zhang, B. Quan, W. Xu, H. Du, D. Xie, and Y. Chen, "Electrically triggered VO2 reconfigurable metasurface for amplitude and phase modulation of terahertz wave," *Journal of Lightwave Technology*, Vol. 39, No. 11, 3488–3494, 2021.

[118] Pan, W.-M., J.-S. Li, and C. Zhou, "Switchable digital metasurface based on phase change material in the terahertz region," *Optical Materials Express*, Vol. 11, No. 4, 1070–1079, 2021.

[119] Xiao, B., Y. Zhang, S. Tong, J. Yu, and L. Xiao, "Novel tunable graphene-encoded metasurfaces on an uneven substrate for beam-steering in far-field at the terahertz frequencies," *Optics Express*, Vol. 28, No. 5, 7125–7138, 2020.

[120] Xu, J., W. Liu, and Z. Song, "Terahertz dynamic beam steering based on graphene coding metasurfaces," *IEEE Photonics Journal*, Vol. 13, No. 4, 1–9, 2021.

[121] Kwon, D., S. Kim, K. Park, S. Kim, H. Kim, H. Yang, S. Bang, and J. Oh, "Field evaluation of reconfigurable intelligent surface with varying surface size," in *2023 IEEE International Symposium on Antennas and Propagation and USNC-URSI Radio Science Meeting (USNC-URSI)*, 17–18, Portland, OR, USA, 2023.

[122] Buchnev, O., N. Podoliak, K. Kaltenecker, M. Walther, and V. A. Fedotov, "Metasurface-based optical liquid crystal cell as an ultrathin spatial phase modulator for THz applications," *ACS Photonics*, Vol. 7, No. 11, 3199–3206, 2020.

[123] Wu, J., Z. Shen, S. Ge, B. Chen, Z. Shen, T. Wang, C. Zhang, W. Hu, K. Fan, W. Padilla, Y. Lu, B. Jin, J. Chen, and P. Wu, "Liquid crystal programmable metasurface for terahertz beam steering," *Applied Physics Letters*, Vol. 116, No. 13, 131104, 2020.

[124] Liu, C. X., F. Yang, X. J. Fu, J. W. Wu, L. Zhang, J. Yang, and T. J. Cui, "Programmable manipulations of terahertz beams by transmissive digital coding metasurfaces based on liquid crystals," *Advanced Optical Materials*, Vol. 9, No. 22, 2100932, 2021.

[125] Shen, Y., J. Wang, Q. Wang, X. Qiao, Y. Wang, and D. Xu, "Broadband tunable terahertz beam deflector based on liquid crystals and graphene," *Crystals*, Vol. 11, No. 9, 1141, 2021.

[126] Chen, D., J. Yang, J. Huang, Z. Zhang, W. Xie, X. Jiang, X. He, Y. Han, Z. Zhang, and Y. Yu, "Continuously tunable metasurfaces controlled by single electrode uniform bias-voltage based on nonuniform periodic rectangular graphene arrays," *Optics Express*, Vol. 28, No. 20, 29 306–29 317, 2020.

[127] Lin, S., B. Zheng, G. C. Alexandropoulos, M. Wen, M. Di Renzo, and F. Chen, "Reconfigurable intelligent surfaces with reflection pattern modulation: Beamforming design and performance analysis," *IEEE Transactions on Wireless Communications*, Vol. 20, No. 2, 741–754, 2021.

[128] Jamshed, M. A., A. Nauman, M. A. B. Abbasi, and S. W. Kim, "Antenna selection and designing for THz applications: Suitability and performance evaluation: A survey," *IEEE Access*, Vol. 8, 113 246–113 261, 2020.

[129] El Mossallamy, M. A., H. Zhang, L. Song, K. G. Seddik, Z. Han, and G. Y. Li, "Reconfigurable intelligent surfaces for wireless communications: Principles, challenges, and opportunities," *IEEE Transactions on Cognitive Communications and Networking*, Vol. 6, No. 3, 990–1002, 2020.

[130] Alexandropoulos, G. C., G. Lerosey, M. Debbah, and M. Fink, "Reconfigurable intelligent surfaces and metamaterials: The potential of wave propagation control for 6G wireless communications," *arXiv preprint arXiv:2006.11136*, 2020.

[131] Zhao, Y., "Reconfigurable intelligent surfaces for 6G: Applications, challenges, and solutions," *Frontiers of Information Technology & Electronic Engineering*, Vol. 24, No. 12, 1669–1688, 2023.

[132] Karahan, S. N., A. G. Toprak, O. B. Mercan, and Y. E. Tok, "The evolution of wireless communication with the THz spectrum: New horizons in 6G," in *2025 3rd Cognitive Models and Artificial Intelligence Conference (AICCONF)*, 1–7, Prague, Czech Republic, 2025.

[133] Aghabeyki, P., Y. Cai, G. Deng, Z.-H. Tan, and S. Zhang, "A dual-polarized reconfigurable reflectarray with a thin liquid crystal layer and 2-D beam scanning," *IEEE Transactions on Antennas and Propagation*, Vol. 71, No. 4, 3282–3293, 2023.

[134] Rahim, J., P.-F. Li, S.-W. Qu, and S. Hussain, "Wideband and wide-angle scanning patch array antenna with substrate cavity and parasitic layer integration," *IEEE Antennas and Wireless Propagation Letters*, Vol. 25, No. 1, 164–168, 2026.

[135] Chang, C.-Y. and H.-T. Chou, "A millimeter-wave binary reconfigurable intelligent surface on a low-cost FR4 substrate," in *2024 18th European Conference on Antennas and Propagation (EuCAP)*, 1–4, Glasgow, United Kingdom, 2024.

[136] Xu, H., S. Xu, F. Yang, and M. Li, "Design and experiment of a dual-band 1 bit reconfigurable reflectarray antenna with independent large-angle beam scanning capability," *IEEE Antennas and Wireless Propagation Letters*, Vol. 19, No. 11, 1896–1900, 2020.

[137] Yang, F., K. Ma, and M. Li, "Wideband, wide-angle scanning active reconfigurable intelligent surface," in *2025 IEEE MTT-S International Wireless Symposium (IWS)*, 1–3, Xi'an, China, 2025.

[138] Fonseca, F. H. S., G. I. Morais, G. C. Clemente, and C. J. B. Pagan, "Tunable 2-bit unit cell based in a square loop for reconfigurable intelligent surface application," in *2022 Asia-Pacific Microwave Conference (APMC)*, 875–877, Yokohama, Japan, 2022.

[139] Araghi, A., M. Khalily, M. Safaei, A. Bagheri, V. Singh, F. Wang, and R. Tafazolli, "Reconfigurable intelligent surface (RIS) in the sub-6 GHz band: Design, implementation, and real-world demonstration," *IEEE Access*, Vol. 10, 2646–2655, 2022.

[140] Da Silva, L. G., Z. Chu, P. Xiao, and A. C. Sodré Jr., "A varactor-based 1024-element RIS design for mm-waves," *Frontiers in Communications and Networks*, Vol. 4, 1086011, 2023.

[141] Abrardo, A., A. Toccafondi, and M. Di Renzo, "Analysis and optimization of reconfigurable intelligent surfaces based on S-parameters multiport network theory," in *2024 18th European Conference on Antennas and Propagation (EuCAP)*, 1–4, Glasgow, UK, 2024.

[142] Vabichevich, D., A. Belov, and A. Sayanskiy, "Suppression of quantization lobes in 1-bit reconfigurable intelligent surfaces," *IEEE Antennas and Wireless Propagation Letters*, Vol. 22, No. 12, 2808–2811, 2023.

[143] Hao, Y., C. Deng, X. Cao, Y. Yin, and K. Sarabandi, "A high aperture efficiency 1-bit reconfigurable reflectarray antenna with extremely low power consumption," *IEEE Transactions on Antennas and Propagation*, Vol. 72, No. 1, 1015–1020, 2024.

[144] Chen, L., K. L. Chung, G. Lai, J. Yao, X. Zou, X. Cheng, K. Zheng, and Y. Li, "Cross deployment of active and passive reconfigurable intelligent surfaces (RISs) for next-generation communications," in *2022 IEEE 5th International Conference on Electronic Information and Communication Technology (ICEICT)*, 829–831, Hefei, China, 2022.

[145] Zhang, Z., L. Dai, X. Chen, C. Liu, F. Yang, R. Schober, and H. V. Poor, "Active RIS vs. passive RIS: Which will prevail in 6G?" *IEEE Transactions on Communications*, Vol. 71, No. 3, 1707–1725, 2023.

[146] Liu, K., Z. Zhang, L. Dai, S. Xu, and F. Yang, "Active reconfigurable intelligent surface: Fully-connected or sub-connected?" *IEEE Communications Letters*, Vol. 26, No. 1, 167–171, 2022.

[147] Kolomvakis, N. and E. Björnson, "Nonlinear distortion issues created by active reconfigurable intelligent surfaces," in *2024 18th European Conference on Antennas and Propagation (EuCAP)*, 1–5, Glasgow, UK, 2024.

[148] Van Veen, B. D. and K. M. Buckley, "Beamforming: A versatile approach to spatial filtering," *IEEE Assp Magazine*, Vol. 5, No. 2, 4–24, 1988.

[149] Björnson, E., □. Özdogan, and E. G. Larsson, "Reconfigurable intelligent surfaces: Three myths and two critical questions," *IEEE Communications Magazine*, Vol. 58, No. 12, 90–96, 2020.

[150] Singh, K., P.-C. Wang, S. Biswas, S. K. Singh, S. Mumtaz, and C.-P. Li, "Joint active and passive beamforming design for RIS-aided IBFD IoT communications: QoS and power efficiency considerations," *IEEE Transactions on Consumer Electronics*, Vol. 69, No. 2, 170–182, 2023.

[151] Siddiqi, M. Z., R. Mackenzie, M. Hao, and T. Mir, "On energy efficiency of wideband RIS-aided cell-free network," *IEEE Access*, Vol. 10, 19 742–19 752, 2022.

[152] Hong, I.-P., "Reviews based on the reconfigurable intelligent surface technical issues," *Electronics*, Vol. 12, No. 21, 4489, 2023.

[153] Kashyap, B. G., P. C. Theofanopoulos, Y. Cui, and G. C. Trichopoulos, "Mitigating quantization lobes in mmWave low-bit reconfigurable reflective surfaces," *IEEE Open Journal of Antennas and Propagation*, Vol. 1, 604–614, 2020.

[154] Yin, J., Q. Wu, Q. Lou, H. Wang, Z. N. Chen, and W. Hong, "Single-beam 1 bit reflective metasurface using prephased unit cells for normally incident plane waves," *IEEE Transactions on Antennas and Propagation*, Vol. 68, No. 7, 5496–5504, 2020.

[155] Chen, X. Y., J. C. Ke, W. Tang, *et al.*, "Design and implementation of MIMO transmission based on dual-polarized reconfigurable intelligent surface," *IEEE Wireless Communications Letters*, Vol. 10, No. 10, 2155–2159, 2021.

[156] Jiao, H., H. Liu, and Z. Wang, "Reconfigurable intelligent surfaces aided wireless communication: Key technologies and challenges," in *2022 International Wireless Communications and Mobile Computing, IWCMC 2022*, 1364–1368, Dubrovnik, Croatia, 2022.

[157] Rafique, A., N. U. Hassan, I. H. Naqvi, M. Q. Mehmood, and M. Zubair, "Benchmarking framework for reconfigurable intelligent surfaces," in *2021 IEEE Global Communications Conference (GLOBECOM)*, Madrid, Spain, 2021.

[158] Rana, B., S. S. Cho, and I. P. Hong, "Review paper on hardware of reconfigurable intelligent surfaces," *IEEE Access*, Vol. 11, 29 614–29 634, 2023.